Optimal Interventions in Networks during a Pandemic

Roland Pongou[1], Guy Tchuente[2*†] and Jean-Baptiste Tondji[3†]

[1]Department of Economics, University of Ottawa, 120 University Private, Social Sciences Building, Ottawa, K1N 6N5, Ontario, Canada.

[2]School of Economics, University of Kent, Kennedy Building, Park Wood Road, Canterbury, CT2 7FS, Kent, United Kingdom.

[3*]Department of Economics, The University of Texas Rio Grande Valley, 1201 West University Drive, Edinburg, 78539, Texas, United States.

*Corresponding author(s). E-mail(s): g.tchuente@kent.ac.uk;
Contributing authors: rpongou@uottawa.ca;
jeanbaptiste.tondji@utrgv.edu;
†These authors contributed equally to this work.

Abstract

We develop a model of optimal lockdown policy for a social planner who balances population health with short-term wealth accumulation. The unique solution depends on tolerable infection incidence and social network structure. We then use unique data on nursing home networks in the United States to calibrate the model and quantify state-level preference for prioritizing health over wealth. We also empirically validate simulation results derived from comparative statics analyses. Our findings suggest that policies that tolerate more virus spread (laissez-faire) increase state GDP growth and COVID-19 deaths in nursing homes. The detrimental effects of laissez-faire policies are more potent for nursing homes that are more peripheral in networks, nursing homes in poorer counties, and nursing homes that operate on a for-profit basis. We also find that U.S. states with Republican governors have a higher tolerable incidence level, but these policies tend to converge with a high death count.

Keywords: COVID-19, Health-vs-wealth prioritization, Lockdown, Networks, Nursing homes

JEL Classification: D85 , E61 , H12 , I18 , J15

1 Introduction

In this study, we develop a theory of optimal lockdown policy for a social planner who prioritizes population health over short-term wealth accumulation during a pandemic that spreads through networks of physical contacts. Using unique data on nursing home networks in the United States, we calibrate the model and quantify state-level preference for prioritizing health over wealth during the COVID-19 pandemic. We also uncover new results on the effects of network configuration, network centrality, and health policies on COVID-19 deaths in nursing homes.

The application of our model to the spread of COVID-19 is timely and fitting. COVID-19 has affected millions of individuals and claimed many lives globally. To reduce its spread, governments worldwide have relied massively on lockdown and social distancing policies (Buchholz, 2020). While lockdown measures have had some positive results, the associated economic costs have been considerable (Marquez-Padilla & Saavedra, 2022). The gross domestic product in both developed and developing countries has decreased significantly as a result of economic contraction (International Monetary Fund, 2020). The significant costs associated with quasi-complete lockdowns have forced governments to think about alternative policies that are less costly, such as imposing quarantine measures only on certain individuals while letting others go back to work. The natural questions that arise are: how do we design optimally targeted lockdown policies that account for social network structure, and how do these policies affect health and economic dynamics?

We address these questions for a society that, to a certain extent, prioritizes health over short-term wealth accumulation.[1] The problem is formalized using an N-SIRD model with lockdown as follows. Agents (including individuals and social infrastructures) are connected through a weighted undirected network of physical contacts through which the virus is likely to spread. At any point in time, an agent is in one of the following health compartments: susceptible (S), infected (I), recovered (R), and dead (D). Susceptible agents can become infected, while infected agents can recover or die. To reduce the contagion, a social planner enforces a lockdown which modifies the structure of the prevailing social network. Susceptible, infected and recovered agents can all be sent into lockdown at different individual probabilities. The disease dynamics follow an individual-based mean-field model for epidemic modeling

[1] Our assumption that health is prioritized over short-term economic prosperity is consistent with recent observations; e.g., Heap, Koop, Matakos, Unan, and Weber (2020), and Stiglitz (2020). For instance, Stiglitz wrote that: "There can be no economic recovery until the virus is contained, so addressing the health emergency is the top priority for policymakers." (Stiglitz, 2020, n.d).

on networks.[2] The planner's objective is to determine the lockdown policy that contains the spread of the disease below a tolerable infection incidence level, and that maximizes the present discounted value of real income (or alternatively, that minimizes the economic cost of the pandemic), in that order of priority. In other words, the social planner can allocate the "work-from-home" rights to achieve these goals.

An appeal of our approach to the social planner's problem is that it does not force us to assign a precise monetary value to health or to life.[3] Rather, it allows some flexibility in how to design policies, with clear health and economic goals in mind. For instance, the social planner could set an infection incidence level that allows to keep the number of infected individuals below hospitals' maximum capacities. We apply our theoretical model to analyze: (1) the effect of network structure on the dynamics of optimal lockdown, infection, recovery, death, and economic costs; (2) the tradeoff between public health and wealth accumulation; and (3) how different measures of network centrality affect the probability of being sent to lockdown.

To solve the planner's problem, we first characterize the disease dynamics in our epidemiological model and obtain a unique solution under classical conditions. Proposition 1 shows that the rates of infection, recovery, and death at any given time are functions of the lockdown variable and the initial network of contacts that captures social structure. Proposition 3 shows that the planner's problem admits a unique solution that depends on both the infection incidence level tolerated by the planner and the prevailing network of physical contacts that characterizes the society. Proposition 3 also shows that the tolerable infection incidence level and the network of physical contacts determine the disease dynamics and the economic costs of lockdown. Furthermore, Proposition 2 illustrates the role of the basic reproduction number, R_0, in enforcing mitigation strategies, including lockdown, when facing a potential virus spread.[4] Proposition 4 demonstrates that these lockdown policies affect the total number of individuals experiencing infection during the outbreak.

Using simulations which rely on realistic early COVID-19 transmission rate data, we conduct several comparative static analyses of our theoretical findings. Our results in Fig. 1 show that a higher tolerable incidence level results in lower lockdown rates and a smaller loss in economic surplus. While this finding illustrates the health-vs-wealth tradeoff the social planner faces, it does not prescribe any resolution since the planning decision depends on the relative value assigned to population health and short-term economic conditions by society. We also illustrate how lattice, small-world, random, and scale-free network structures affect optimal lockdown probabilities and disease dynamics,

[2] We refer to Pastor-Satorras, Castellano, Van Mieghem, and Vespignani (2015) for an excellent survey on these models.

[3] See, e.g., Pindyck (2020) and Bosi, Camacho, and Desmarchelier (2021) for the expression of a similar concern. In the same perspective, Pestieau and Ponthière (2022) examine how designing optimal lockdown strategies under different social welfare criteria when planners face a problematic trade-off between saving lives and prosperity during a pandemic.

[4] R_0 represents the expected number of secondary infectious produced by a primary case introduced in a fully susceptible population (Anderson & May, 1992).

respectively. Our simulation results in Fig. 3 show that the cumulative proportion of the population sent into lockdown is always higher in random and small-world network structures than in lattice and scale-free structures. These lockdown policies translate to different epidemic and economic cost dynamics for each network. We extend our analysis to examine the potential impact of *network density* (or the interconnections between agents in a network) in our N-SIRD model for a small-world network. Our simulations in Fig. 4a show that optimal lockdown probabilities increase with network density.[5] Third, we illustrate how measures of network centrality affect optimal lockdown probabilities and disease dynamics. Table 1 provides the correlations between four network metrics—degree, eigenvector, betweenness, and closeness—and the average lockdown probabilities in a small-world network. Our simulation results suggest that individuals that are more central in such a network are more likely to be sent into lockdown. This implies that more restrictive lockdown policies have a greater effect on individuals that are more central in networks. We provide a discussion of the robustness of these findings in Section 4.3. Overall, our simulation results confirm the intuition that not *all* agents should be placed into full lockdown under the optimal policy; e.g., Gollier (2020a), Gollier (2020b), Acemoglu, Chernozhukov, Werning, and Whinston (2021), Bosi et al. (2021), Chang et al. (2021), and Pestieau and Ponthière (2022). This planning decision is justified since the goal in the N-SIRD model is to disconnect the prevailing contact network while, contrary to a purely epidemiological model, maintaining economic activities to the greatest extent possible.

We calibrate our model and test some of its key predictions using unique U.S. nursing home networks data. The senior population in the U.S. accounts for a significant share of America's COVID-19 deaths (Conlen et al., 2021; National Center for Health Statistics, 2020). The surge of COVID-19 cases and deaths in nursing homes led the American federal government to ban nursing home visits on March 13th, 2020. This restriction enabled researchers from the "Protect Nursing Homes" project to construct a U.S. nursing homes network, using smartphone data (M.K. Chen, Chevalier, & Long, 2021). We use this network data in conjunction with other nursing home and U.S. state-level datasets to calibrate the N-SIRD model.[6] This calibration allows us to estimate the value of the tolerable COVID-19 infection incidence level (λ) for 26 U.S. states. The parameter λ estimates the state government's tolerable COVID-19 infection incidence, which by assumption represents the relative value the state assigns to population health and economic prosperity. As such, a higher value of λ describes a policy that tends more towards a "laissez-faire" regime (Gollier, 2020a), indicating a planner's inclination to maximize short-term economic gains. We find that the tolerable infection incidence level varies significantly across U.S. states, making it possible to test some theoretical predictions of our model. Our analysis in Section 5.1.2 suggests that we can attribute variations in λ to interstate heterogeneity and differences in states' demographic and

[5] Our series of robustness checks conjecture that the simulation results with lattice, random, and scale-free networks are qualitatively consistent with those obtained with the small-world network.

[6] We refer the reader to Section 5.1.1 for other data sources.

political characteristics, including the gender of a state's governor, the party affiliation of a state's governor, a state's geographic location, and the number of COVID-19 fatalities in a state. These findings complement other studies showing an association between the political affiliation of a U.S. state's governor and COVID-19 cases and deaths (e.g., Neelon, Mutiso, Mueller, Pearce, and Benjamin-Neelon (2021), and Baccini and Brodeur (2021)).

Using regression-based analyses, we find that laissez-faire policies are associated with more COVID-19 deaths, consistent with the results from the simulation analysis. Nursing homes that are more central in the network experience more COVID-19 deaths. However, laissez-faire policies are more harmful to nursing homes that are more peripheral in the network. We also find that the detrimental effect of laissez-faire policies on COVID-19 fatalities in nursing homes is potent in poorer counties and in for-profit nursing homes. Our results are robust to the inclusion of an array of nursing home and U.S. state-level control variables, such as overall nursing home quality and county fixed effects. In another empirical test of the N-SIRD model with lockdown, we investigate the relationship between U.S. states' tolerable infection incidence level for COVID-19 and the state's GDP growth for 2020. We find that laissez-faire policies are associated with higher GDP growth, consistent with our simulation results. The analysis controls several factors, including the party affiliation and gender of the U.S. state's governor. Interestingly, we find that the positive economic effect of laissez-faire policies is reduced for U.S. states with a democratic governor.

Our paper contributes to several literatures. The epidemiological framework that we use to model the planning problem is a continuous-time individual-based mean-field model which belongs to the class of theoretical approaches for epidemic modeling on undirected heterogeneous networks; Pastor-Satorras et al. (2015) provide a review of these epidemiological models. This literature includes a class of mean-field models (Barabási, Albert, & Jeong, 1999; Green, Kiss, & Kao, 2006; Kephart & White, 1992) and N-intertwined models via Markov theory in both discrete time (Ganesh, Massoulié, & Towsley, 2005; Wang, Chakrabarti, Wang, & Faloutsos, 2003) and continuous time (Van Mieghem, Omic, & Kooij, 2008). Asavathiratham (2001) and Garetto, Gong, and Towsley (2003) review other general models for virus spread in networks based on Markov theory. These models extend the classical susceptible-infected-recovered (SIR) (Kermack & McKendrick, 1927) and SIRD (Hethcote, 2000) epidemic processes to heterogeneous networks. To this literature, we add a reversible lockdown state to model disease dynamics in an SIRD-epidemic framework. The targeted lockdown policy allows the planner to achieve specific health and economic goals. In this perspective, our study contributes to the literature interacting epidemiology and economics to address a variety of issues.

Recent studies include, among others, Karaivanov (2020) who examines the transmission of COVID-19 through a dynamic social-network model embedding the SIR model onto a graph of network contacts, Bethune and Korinek

(2020) who study the externalities associated with public health interventions in susceptible-infected-susceptible (SIS) and SIR models of infectious disease, Acemoglu et al. (2021) who propose a multi-risk SIR model, Berger, Herkenhoff, Huang, and Mongey (2020), Federico and Ferrari (2020), Gollier (2020b), Prem et al. (2020), Alvarez, Argente, and Lippi (2021), Bandyopadhyay, Chatterjee, Das, and Roy (2021), Bisin and Moro (2021), Eichenbaum, Rebelo, and Trabandt (2021), and Ma et al. (2021) who analyze optimal non-pharmaceutical controls in SIR models, Chang et al. (2021) who use Google mobility data to construct mobility network and metapopulation susceptible–exposed–infectious–removed (SEIR) models to explain differences in COVID-19 fatalities and to inform reopening decisions in ten large U.S. metropolitan areas, and Harris (2020) and Kuchler, Russel, and Stroebel (2021) who document the importance of social media networks (e.g., Facebook) in the selection of targeted lockdown policies. While our model contains some ingredients from each of these other approaches, it differs by incorporating them into a classical model with two key elements, namely a lockdown variable and a weighted network of contacts that is not necessarily *random*. In this weighted network, we also assume that agents are heterogeneous with respect to the intensity of their connections and their individual characteristics. Most importantly, we introduce a *lexicographic approach* to the planning problem.

In this study, our goal is to provide a dynamic economic and epidemiological model of lockdown, in which a planner must choose a lockdown policy which keeps infections below a certain threshold level at the minimum economic cost. Contrary to Bosi et al. (2021), who proposes a model where the planner imposes a single lockdown policy which remains constant over time, we propose a model where lockdown policy is dynamic, reversible, and subject to change over time. In this respect, our model is more in line with Gollier (2020a), Acemoglu et al. (2021), Alvarez et al. (2021), and Pestieau and Ponthière (2022).[7] Assuming an irreversible lockdown under a tractable epidemiological model enables the researcher to derive a closed-form solution while establishing the convexity of the problem with second-order conditions (Bosi et al., 2021; Seierstad & Sydsaeter, 1986). As in Alvarez et al. (2021), the interactions between dynamic lockdown policies and our N-SIRD epidemiological model may make the planner's problem non-convex. Therefore, we cannot use second-order conditions to verify whether a given candidate policy is an optimal solution. In other words, it would not be possible to prove that our optimal lockdown policy is indeed minimizing the economic costs of lockdown. Though we do not address the convexity issue, we follow Alvarez et al. (2021) and Acemoglu et al. (2021) and use simulations to conduct comparative statics analyses within our framework. In addition, we provide an empirical application of the simulation results.

Our study is also connected to the economic literature on the design of optimal interventions in networks and the diffusion of knowledge or contagion via a network. Ballester, Calvó-Armengol, and Zenou (2006) and Banerjee,

[7] We thank an anonymous referee for bringing this issue to our attention.

Chandrasekhar, Duflo, and Jackson (2013) examine the optimal targeting of key players (or the first individuals to receive an information) in a network, while Galeotti, Golub, and Goyal (2020) analyze an optimal intervention of a social planner acting on individual incentives in networks. The choice of an optimal lockdown policy in the social planner problem differentiates our model from these studies by analyzing optimal interventions in a network structure. In our model the choice of lockdown strictness operates to control the spread of infection through the network. Thus, it relates to the studies of Young (2009) and Young (2011) who investigate the diffusion of innovations through a network. Our work is also connected to the models of social learning dynamics in Buechel, Hellmann, and Klößner (2015) and Battiston and Stanca (2015), with the main difference being that infection diffusion is exogenous in these models. Our epidemiological model also complements and extends Peng, Yang, Zhang, Zhuge, and Hong (2020), by allowing for diffusion dynamics similar to Lloyd, Valeika, and Cintrón-Arias (2006). Additionally, since our network structure is not necessarily random, we are able to develop new applications. Although we only apply our model to the current COVID-19 crisis, we believe that our theory has implications for other infections that spread through physical contacts. In line with Pongou and Serrano (2013), Chang et al. (2021), Fajgelbaum, Khandelwal, Kim, Mantovani, and Schaal (2021), Debnam Guzman, Mabeu, and Pongou (2022), and Pongou, Tchuente, and Tondji (2022), our study also contributes to the growing literature investigating the importance of network structure in the distributional effects of virus spread.

The remainder of this study is organized as follows. Section 2 presents the N-SIRD model with lockdown. Section 3 describes and solves the planning problem. Section 4 uses simulations to provide comparative statics analyses of our theoretical findings. Section 5 provides an empirical application of the theoretical model. Section 6 discusses some policy implications and offers concluding remarks. The Appendices contain complementary information for the N-SIRD model and additional simulation and empirical results.

2 N-SIRD Model with the Lockdown

We describe the evolution of an epidemic that spreads through an undirected weighted and symmetric network of physical contacts, A. Time t is continuous, $t \in [0, \infty)$, and there is no vital dynamics so that a community of size N is constant through time: $N(t) = N$ for all t.

Social network structure.

We represent A by the adjacency matrix $(A_{i,j})$, where $A_{ij} = A_{ji} \in [0, \infty)$ represents the *weight* or *intensity* at which individuals i and j are connected in A, with $A_{ij} = 0$ if $i = j$. The intensity of connections is the primary source of heterogeneity between agents in the social network structure A.[8]

[8]Some studies exploring virus spread in networks consider that nodes with the same number of connections are equivalent. Then, instead of working with quantities specifying the state of each node $i \in N$ (as we do throughout), the relevant variables specify the state of all nodes

However, other characteristics may differentiate agents with the same number of connections. In Section 5, in which we apply our theory to U.S. nursing home networks (M.K. Chen et al., 2021), a node is defined as a single nursing home. As such, nodes (nursing homes) have different surplus functions and can be either for-profit or not-for-profit.

Health compartments.

At any time t, individuals are divided into four compartments: susceptible $S(t)$, infected $I(t)$, recovered $R(t)$, and deceased $D(t)$, where $S(t) + I(t) + R(t) + D(t) = N$. For simplicity, we drop the time subscript of different compartments. Each individual i is in each of the four different compartments with the following probabilities: $s_i = P(i \in S)$, $x_i = P(i \in I)$, $r_i = P(i \in R)$, and $d_i = P(i \in D)$, with $s_i + x_i + r_i + d_i = 1$.

Lockdown.

We incorporate a lockdown variable to capture the fact that a social planner might decide to reduce the spread of the infection by enforcing a lockdown policy. This lockdown policy reduces the spread of infection by modifying the existing social network structure, A. Let L denote the lockdown state that is controlled by the social planner, and $l_i = P(i \in L)$ denote the probability that a random individual i is sent into lockdown, with $l_i = 1$ designating full lockdown and $l_i = 0$ no lockdown. Intermediate values of $l_i \in (0, 1)$ represent less extreme cases.

Virus spread.

Susceptible individuals may become infected by coming into contact with infected individuals at a constant passing rate β. Individuals move from susceptible to infected, then either recover at rate γ or die at rate κ.[9] We assume that a policy of full lockdown is 100% effective in curbing the contagion, i.e., full lockdown is similar to self-isolation.[10] An individual in full lockdown is completely disconnected from all contacts. Thus, susceptible individuals in full lockdown in period t remain susceptible in the next period $t+\epsilon$, ϵ positive and very small. Therefore, with lockdown, the probability of an individual i being infected is equal to the probability that they are susceptible (s_i) and not sent

with the same number of connections. For more details, we refer to a review of degree mean-field models by Pastor-Satorras et al. (2015). Other recent studies consider partitioning individuals into different risk groups following age or stage structured compartmental epidemiological models; e.g., Acemoglu et al. (2021), and Pestieau and Ponthière (2022).

[9]Our assumption of constant transmission rates β, γ, and κ follows the canonical SIR and SIRD epidemiological models. Recent studies apply these models to analyze the possible COVID-19 outcomes; e.g., Anastassopoulou, Russo, Tsakris, and Siettos (2020), Acemoglu et al. (2021), and Alvarez et al. (2021). We note that, unlike our framework which considers a fixed contact rate β, other studies tend to use time-varying contact rates when examining optimal public health interventions, such as lockdown and social distancing policies; e.g., Gollier (2020b).

[10]Our assumption of full effectiveness is contrary to Alvarez et al. (2021) who considers the case where full lockdown is only partially effective in eliminating the transmission of the virus. Alvarez et al. justify this limitation by the fact that people can still interact in full lockdown. We assume that being in full lockdown severs the agent's contacts with all neighbors in the prevailing network.

into full lockdown $(1 - l_i > 0)$ multiplied by the probability that a neighbor j is infected $(x_j > 0)$ and is not sent into full lockdown $(1 - l_j > 0)$, scaled by the connection intensity between i and j $(A_{ij} > 0)$ and the contact rate β. It follows that the infinitesimal change in infection probabilities over time for individual i is:

$$\dot{x_i} = \beta s_i(1 - l_i) \sum_{j \in N} A_{ij}(1 - l_j)x_j - (\gamma + \kappa)x_i.$$

Disease Dynamics.

The equation generated by $\dot{x_i}$ describes the law of motion of the infection probabilities for individual i. Any individual can be sent into lockdown regardless of whether the individual is susceptible, infected or recovered. For each $i \in N$, let $X_i = (x_i, s_i, r_i, d_i)^T$ denote agent i's health characteristics in the population, where T means "transpose." We summarize the laws of motion of the variables of interest given the lockdown profile $l = (l_i)_{i \in N}$ by the following nonlinear system of ordinary differential equations:

$$\text{(ODE)} : \begin{cases} \dot{x_i} = \beta s_i(1 - l_i) \sum_{j \in N} [A_{ij}(1 - l_j)x_j] - (\gamma + \kappa)x_i \\ \dot{s_i} = -\beta s_i(1 - l_i) \sum_{j \in N} [A_{ij}(1 - l_j)x_j] \\ \dot{r_i} = \gamma x_i \\ \dot{d_i} = \kappa x_i \\ s_i + x_i + r_i + d_i = 1 \end{cases}$$

where the initial value point $(x_i(0), s_i(0), r_i(0), d_i(0))$ is such that

$$x_i(0) \geq 0,\ s_i(0) \geq 0,\ r_i(0) \geq 0,\ d_i(0) \geq 0, \text{ and } x_i(0) + s_i(0) + r_i(0) + d_i(0) = 1.$$

We use the N-SIRD model with lockdown (ODE) to obtain qualitative insights into the transmission dynamics of the disease. Before using the model to simulate disease dynamics and evaluate control strategies in Sections 4 and 5, respectively, it is instructive to explore the model's basic qualitative properties. First, we must establish that a solution for the system (ODE) exists. We demonstrate the existence of a solution for the system (ODE) in Proposition 1.

Proposition 1 *The system (ODE) admits a unique solution* $\mathcal{S}^* = \mathcal{S}^*(l, A, \beta, \gamma, \kappa)$.

Proof See Appendix C.1. □

Next, we carry out the analysis of the N-SIRD model in the feasible domain:

$$\Omega = \{((x_i)_{i\in N}, (s_i)_{i\in N}, (r_i)_{i\in N}, (d_i)_{i\in N}) \in [0,1]^{4n} : x_i + s_i + r_i + d_i \leq 1, 1 \leq i \leq n\}.$$

The domain Ω is positively invariant (i.e., solutions that start in Ω remain in Ω for all $t \geq 0$). Hence, we can confirm that the system (ODE) is mathematically and epidemiologically well posed in Ω (Hethcote, 2000).

Equilibria and the basic reproduction number.

To find equilibria in the system (ODE), we set each expression on the left-hand side of equations in (ODE) equal to zero. It follows that any equilibrium point constitutes a disease free equilibrium point (DFE) in which the probability of infection is zero, i.e., $x_i = 0$ for all $i \in N$. For simplicity, we analyse the disease dynamics at the DFE $E_0 = (0, ..., 0, 1, ..., 1, 0, ...0, ..., 0)$ in a completely susceptible population. One of the most fundamental concepts in epidemiology is the basic reproduction number, R_0. The number, R_0, describes the expected number of secondary cases produced by a typical infected individual during their entire period of infectiousness in a completely susceptible population. Following Diekmann, Heesterbeek, and Metz (1990) and Van den Driessche and Watmough (2002), only those in the infected compartments I are used in the calculation of R_0. We use the next-generation matrix method to calculate R_0. Formally, R_0 is defined as the spectral radius of the next-generation matrix $\mathcal{A}\mathcal{B}^{-1}$, where $\mathcal{A}$ is the matrix of the rate of generation of new infections, and $\mathcal{B}$ is the matrix of transfer of individuals among the four health compartments. Following Van den Driessche and Watmough (2002), from the system (ODE), we write:

$$\dot{x_i} = \mathcal{A}_i - \mathcal{B}_i, \text{ where}$$
$$\mathcal{A}_i = \beta(1 - x_i - r_i - d_i)(1 - l_i) \sum_{j\in N} [A_{ij}(1 - l_j)x_j], \text{ and } \mathcal{B}_i = (\gamma + \kappa)x_i.$$

$\mathcal{A}$ is the Jacobian matrix, and it is given by $\mathcal{A} = [\frac{\partial \mathcal{A}_i}{\partial x_j} = \mathcal{A}_{ij}]_{E_0}$, and $\mathcal{B} = [\frac{\partial \mathcal{B}_i}{\partial x_j} = \mathcal{B}_{ij}]_{E_0}$, where $x = (x_j) = (x_1, x_2, ..., x_n)$. We have $\mathcal{A}_{ii} = -\beta(1 - l_i) \sum_{j\in N} [A_{ij}(1 - l_j)x_j]$ and $\mathcal{A}_{ij} = \beta A_{ij}(1 - x_i - r_i - d_i)(1 - l_i)(1 - l_j)$ for $j \neq i$. At the equilibrium point E_0, it holds that $\mathcal{A}_{ii}(E_0) = 0$ and $\mathcal{A}_{ij}(E_0) = \beta A_{ij}(1 - l_i)(1 - l_j)$ for $j \neq i$. Since $A_{ii} = 0$, we can write

$$\mathcal{A}_{ij}(E_0) = \beta A_{ij}(1 - l_i)(1 - l_j), \text{ for } 1 \leq i, j \leq n.$$

It is straightforward to have $\mathcal{B}_{ij}(E_0) = (\gamma + \kappa)\delta^{ij}$, where $\delta^{ij} = 1$ if $i = j$, and $\delta^{ij} = 0$ otherwise. It follows that $\mathcal{B}_{ii} = \gamma + \kappa$ and $\mathcal{B}_{ii}^{-1} = \frac{1}{\gamma+\kappa}$, for all $1 \leq i \leq n$ such that

$$\mathcal{B} = diag(\mathcal{B}_{11}, ..., \mathcal{B}_{ii}, ..., \mathcal{B}_{nn}) \text{ and } \mathcal{B}^{-1} = diag(\mathcal{B}_{11}^{-1}, ..., \mathcal{B}_{ii}^{-1}, ..., \mathcal{B}_{nn}^{-1}).$$

Therefore, $\mathcal{A}\mathcal{B}^{-1} \equiv \mathcal{M} = [\mathcal{M}_{ij}]_{1\leq i,j\leq n}$, where $\mathcal{M}_{ij} = \frac{\beta}{\gamma+\kappa}A_{ij}(1-l_i)(1-l_j)$, and $R_0 = \rho(\mathcal{M}) := \max\{\mathsf{e} : e \text{ is an eigenvalue of } \mathcal{M}\}$. In a fully homogeneous connected society (e.g., a lattice network), it holds that $A_{ij} = 1$ for all agents i and j $(i \neq j)$, and without any non-pharmaceutical intervention such as lockdown, $R_0 = \frac{\beta}{\gamma+\kappa}(n-1)$. Since A is undirected, it holds that $A_{ij} = A_{ji}$, so that $\mathcal{M}_{ij} = \mathcal{M}_{ji}$ for all i and j. Additionally, since all the values A_{ij}, $1-l_i$, and $1-l_j$ are real and non-negative, it follows that $\mathcal{M}$ is a non-negative symmetric real matrix. Therefore, all of its eigenvalues and eigenvectors are real. Since the diagonal of $\mathcal{M}$ consists of zero, it holds that the trace of $\mathcal{M}$ is zero (recall that the trace of $\mathcal{M}$ is the sum of its eigenvalues). Given that the determinant of $\mathcal{M}$, which is the product of its eigenvalues, is not necessarily zero, it follows that R_0 is positive. The following result provides the asymptotic stability analysis of continuum of the disease-free equilibrium E_0.

Proposition 2 *The continuum of DFE E_0 of the system (ODE) is locally-asymptotically stable if $R_0 < 1$, but unstable if $R_0 > 1$.*

Proof See Appendix C.2. □

The epidemiological interpretation of Proposition 2 is that a small invasion of virus-infected agents will not generate an epidemic outbreak in society when the basic reproduction number is below 1. However, when $R_0 > 1$, the epidemic rises to a peak and then eventually declines to zero. Proposition 2 also suggests that a social planner may need lockdown policies to reduce contagion only when R_0 is expected to be greater than 1. For instance, when $R_0 = 2$, one infected agent will, on average, infect two different agents during their period of infectiousness. Following this sequence, we expect each new infected agent to transmit the virus to two other susceptible agents. Therefore, without any intervention and mitigation measures, the contagion may spread exponentially and cause significant health and economic costs. This explains why lockdown and quarantine policies, together with other non-pharmaceutical interventions such as physical distancing, mask wearing, and hygiene measures, are the immediate solutions that policymakers turn to at the onset of any pandemic when pharmaceutical treatments are not available. Proposition 4 in Appendix A illustrates the pivotal role of R_0 and the next-generation matrix $\mathcal{M}$ in determining the final size of the epidemic in the N-SIRD model with the lockdown. In response to a larger size of R_0, enforcing a lockdown state to reduce physical contacts between targeted individuals with other agents in the population changes the disease dynamics in the social network structure. As we will show throughout, such a non-pharmaceutical decision could help planners fight the virus spread at a minimum cost by allowing some agents to continue supplying services in the economy.

3 The Planning Problem: Optimal Lockdown

The unique solution to the nonlinear system (ODE) presented in Section 2 depends on the network structure, A, and the lockdown variable, l. The planning problem consists of choosing the optimal lockdown policy l such that infections are kept below the chosen threshold value at the lowest economic cost possible. Importantly, the planner always *prioritizes* keeping infections under the infection incidence threshold. This means that they are willing to pay an infinitely high economic price to keep infections below their threshold level. Formally, the planner's problem consists of choosing l that:

1. contains the infection *incidence* level (or the relative number of new infections) below a *tolerable* threshold λ; and
2. minimizes the economic costs of the lockdown policy, in that order of priority.

Below, we formalize this lexicographic objective problem.

Containing the spread of infection.

Using $\dot{x_i}$ in the system (ODE), the first objective of the planner is to select a lockdown policy l such that:

$$\dot{x_i} \equiv \dot{x_i}(l) \leq \lambda, \text{ where } \lambda \text{ is a non-negative parameter.} \tag{1}$$

Note that the system (ODE) together with Eq.(1) admits at least one solution. Consider the policy l where each individual is sent into full lockdown, i.e, $l_i(t) = 1$ for all $i \in N$ and t. Then, $\dot{x_i}(l) = -(\gamma + \kappa)x_i$. Therefore, given any $\lambda \geq 0$, it follows that $\dot{x_i}(l) \leq \lambda$. However, this extreme solution induces significant social and economic costs. In practice, the upper bound of the parameter λ could be equal to the basic reproduction number without any lockdown policy, $R_0^v = \rho(\mathcal{M}^v)$, where $\mathcal{M}^v = [\frac{\beta}{\gamma+\kappa}A_{ij}]_{1\leq i,j\leq n}$. Given that lockdown implies a reduction of economic activities, an economically-focused planner might tolerate a value of λ close to R_0^v. In contrast, a cautious (or prudent) planner who prioritizes health over economic prosperity may only tolerate infection incidences λ that fall behind the basic reproduction number R_0.

Minimizing the economic costs of lockdown.

The planner's second-order objective is to minimize the economic costs of lockdown by choosing from the set of policies that satisfy the first objective, the policy that maximizes the present discounted value of aggregate wealth or surplus. To assess the economic effects of lockdown in the population during a pandemic, we consider a simple production economy that we describe as follows.

Inputs. At any given period t, each individual i possesses a capital level k_i, and a labor supply h_i. We assume, as in most SIR models, that individuals

who recover from the infection are immune to the virus and must be released to the workforce. It follows that individuals in compartments S, I, and R are the only potential workers in the economy. The individual labor supply depends on individuals' health compartments and their probability of being in lockdown: $h_i = h_i(s_i, x_i, r_i, d_i, l_i)$, with h_i assumed to be continuous and differentiable in each of its input variables. We assume that h_i is non-decreasing in the probabilities of being susceptible and recovered: $\frac{\partial h_i}{\partial s_i} \geq 0$ and $\frac{\partial h_i}{\partial r_i} \geq 0$. In contrast, labor supply is non-increasing in the probabilities of being infected and deceased and is also non-increasing in lockdown strictness: $\frac{\partial h_i}{\partial x_i} \leq 0$, $\frac{\partial h_i}{\partial d_i} \leq 0$, and $\frac{\partial h_i}{\partial l_i} \leq 0$. Naturally, an individual who is working despite being infected produces less compared to an otherwise identical individual who is healthy. Without loss of generality, we assume that capital is constant over time ($k_i(t) = k_i$, for each t), and labor is a variable input in the production function.

Output. Capital combines with labor to generate output, y_i, based on a production function: $y_i = y_i(k_i, h_i) = y_i(k_i, s_i, x_i, r_i, d_i, l_i)$. We assume that y_i is continuous and differentiable in each of its input variables. Moreover, we make the following natural assumptions: $\frac{\partial y_i}{\partial k_i} \geq 0$, $\frac{\partial y_i}{\partial s_i} \geq 0$, $\frac{\partial y_i}{\partial x_i} \leq 0$, $\frac{\partial y_i}{\partial r_i} \geq 0$, $\frac{\partial y_i}{\partial d_i} \leq 0$, $\frac{\partial y_i}{\partial l_i} \leq 0$, and $\frac{\partial y_i^2}{\partial^2 v} \leq 0$, for each $v \in \{k_i, s_i, x_i, r_i, d_i, l_i\}$. Other important variables in the problem include: the individual cost of one unit of labor (w_i), the price per unit of output (p_i), and the social planner's discount rate (δ).

Aggregate surplus. With the above information, agent i's surplus function, W_i, is given as: $W_i(k_i, s_i, x_i, r_i, d_i, l_i) = p_i y_i(k_i, s_i, x_i, r_i, d_i, l_i) - w_i h_i(s_i, x_i, r_i, d_i, l_i)$. The planner chooses the lockdown profile $l = (l_i)_{i \in N} \in [0, 1]^n$ to maximize the present discounted value of aggregate surplus:

$$W(k, s, x, r, d, l) := \int_0^\infty e^{-\delta t} \left\{ \sum_{i \in N} W_i(k_i, s_i, x_i, r_i, d_i, l_i) \right\} dt$$

$$= \sum_{i \in N} \left\{ \int_0^\infty e^{-\delta t} \left(p_i y_i(k_i, s_i, x_i, r_i, d_i, l_i) - w_i h_i(s_i, x_i, r_i, d_i, l_i) \right) dt \right\}.$$

The social planner's problem.

We recall that $X_i = (x_i, s_i, r_i, d_i)^T$ represents agent i's health characteristics in the population. Given a tolerable infection incidence λ, the planner's task is to choose the optimal admissible lockdown path $l_i^*(t)$, for each agent $i \in N$, in period t, which along with the associated optimal admissible state path $X_i^*(t)$, will maximize the objective functional W. Using optimal control theory, we

can formalize the social planner's problem as:

$$\begin{aligned} &\underset{(l_i)_{i\in N}}{\text{Maximize}} && \int_0^\infty e^{-\delta t} \sum_{i\in N} \{p_i y_i(k_i, s_i, x_i, r_i, d_i, l_i) - w_i h_i(s_i, x_i, r_i, d_i, l_i)\}\, dt \\ &\text{subject to} && \text{(ODE) and } \dot{x_i} \leq \lambda,\ i \in N \\ &\text{and} && l_i(t) \in [0,1] \text{ for all } i \in N \text{ and } t. \end{aligned} \tag{2}$$

We have the following result.

Proposition 3 *The social planner's problem (2) has a unique solution.*

Proof See Appendix C.3. □

Proposition 3 states the existence and uniqueness of a solution to the social planner's problem. In Appendix B, we extend the analysis of problem (2) that proves useful in showing how we obtain our simulated results. Note that determining a closed-form solution to the planning problem (2) is intractable. This is justified by the complex and stochastic nature of the system (ODE) that characterizes our N-SIRD model. To gain some insight into the optimal lockdown policy and the resulting disease and costs dynamics , we follow Alvarez et al. (2021), Acemoglu et al. (2021), and Gollier (2020a), and resort to simulations in Section 4. First, in Section 4.1, we vary the tolerable infection incidence λ to illustrate the tradeoff between health and wealth. Unlike Bosi et al. (2021) who proposes a constant optimal lockdown policy to curve the contagion, our lockdown policy is dynamic, and more in line with Alvarez et al. (2021), Acemoglu et al. (2021), and Gollier (2020a). We differ from Alvarez et al. (2021) and Acemoglu et al. (2021) by not constraining the lockdown probability by an upper bound less than one, which situates our study more in line with Bosi et al. (2021). In our model, a planner could lock down all of society if they found it optimal to do so. However, this case corresponds to a purely epidemiological model and our findings illustrate that full lockdown is not an optimal solution. Second, in Section 4.2, we illustrate how network configuration affects the disease dynamics and their impact on the economy, by changing the nature of the network structure A. Similarly, we also illustrate in Section 4.3 the effects of network centrality on individual lockdown probabilities.

4 Comparative Statics: A Simulation-based Analysis

We choose the parameters in the N-SIRD model to match the dynamics of the infection and early studies on the COVID-19 pandemic and the period in which the researchers at the Protect Nursing Homes gathered the data to build the U.S. nursing home networks. Following Alvarez et al. (2021), we use

data from the World Health Organization (WHO) made public through the Johns Hopkins University Center for Systems Science and Engineering (JHU CCSE). The contact rate β is assumed to be 0.2. The lifetime duration of the virus is assumed to be 18 days (e.g., Acemoglu et al. (2021) and the references therein). Given the information from JHU CCSE access on May 5, 2020, the proportion of recovered closed cases was around 70% for the U.S., 93% for Germany, and 86% for Spain. Thus, we assume that the parameter governing the recovery of an infected patient is given by $\gamma = \frac{0.8}{18}$, and the parameter governing the death dynamics is given by $\kappa = \frac{0.2}{18}$.

Calibrating the production function.

We consider the following functional forms for the labour function (h) and the production function (y):

$$h_i(s_i, x_i, r_i, d_i, l_i) = (1 + \phi_i s_i r_i (1 - x_i)(1 - d_i))(1 - \varphi_i l_i), \tag{3}$$

$$y_i(k_i, s_i, x_i, r_i, d_i, l_i) = k_i^{\alpha_i} h_i^{1-\alpha_i}, \tag{4}$$

where $\phi_i \in [0, 1]$ determines the direct effect on the rate of change in the labor supply when individual i is in one of the natural health compartments, S, I, R and D. The parameter $\varphi_i \in [0, 1]$ represents the direct effect on the labour supply which occurs when individual i is placed in lockdown, with this effect assumed to be non-positive. When $d_i = P(i \in D) = 1$, we should have $l_i = 0$ so that $h_i(s_i, x_i, r_i, 1, 0) = 0$. In Eq. (4), α_i is the elasticity of output with respect to the capital, and $1 - \alpha_i$ is the elasticity of output with respect to labor. The functions h_i in Eq. (3) and y_i in Eq. (4) satisfy the standard conditions mentioned in Section 3.

Our choice of the Cobb-Douglas function as a parametric estimate of the production function is motivated by our empirical analyses in Section 5. Our consideration is also more in line with several studies that argue that the Cobb-Douglas function is a standard parameterization of production functions in the literature (Douglas, 1976), especially in the context of primary care (Wichmann & Wichmann, 2020), and nursing homes (Reyes-Santías, Cordova-Arevalo, & Rivo-Lopez, 2020). Using the recent data collected by M.K. Chen et al. (2021) on U.S. nursing homes, we approximate a typical nursing home's production function as $y_i = k_i^{\alpha_i} h_i^{1-\alpha_i}$, where y_i is the total number of residents (proxies the nursing home's output) who receive care, k_i is the total number of beds (proxies the capital), and h_i is the number of occupied beds (proxies the labor supply). In our simulations, we consider $\alpha_i = \frac{1}{3}$. For more details on our estimation approach of a nursing home's production function, we refer to Appendix F.1.

In all simulations, we consider $\phi_i = 0$ and $\varphi_i = 1$, so that $h_i(s_i, x_i, r_i, d_i, l_i) \approx (1 - l_i)$ and we have a stationary working population. In the context of nursing and long-term care homes, we can justify the labor supply's approximation, $h_i = 1 - l_i$. The connection between two nursing homes is determined by at least one signal received from a smartphone in both houses.

Given the regulatory and staffing structures of U.S. nursing homes, most workers in nursing homes would not be able to work remotely. In the context of our model, this implies that the labour supply will equal zero if a nursing home is in full lockdown, i.e., $h_i = 0$ when $l_i = 1$. The choice $h_i = 1 - l_i$ is therefore an appropriate choice for the labour supply function, since it satisfies all the standard conditions mentioned above and allows for a smooth computational time process in our simulation analyses. Regarding the surplus function, we assume that $w_i = \frac{1}{3}p_i$, for each agent i, and assume that the level of capital is the same for all agents at all time periods. This level of capital is normalized to $k_i = 1$. The annual interest rate is assumed to be equal to 5%. In our simulation analyses, we assume for simplicity that networks are represented by binary adjacent matrices $A = (A_{ij})$, where $A_{ij} = 1$ if agents i and j are connected, and $A_{ij} = 0$, otherwise.[11] In Appendix D, we offer additional explanations of the simulations that we use to conduct our comparative statics analyses.

4.1 Infection Incidence Control and Optimal Lockdown Policy—The Health-vs-Wealth Tradeoff

In our first comparative statics analysis, we illustrate the effect of changing the tolerable infection incidence level on the optimal lockdown policy and describe the tradeoff between maintaining the desired level of population health and minimizing short-term economic costs. We consider an economy of $n = 1000$ agents connected through a *small-world network* (Watts & Strogatz, 1998) with $2 \times n$ edges (A is fixed). In the planning problem, we vary the tolerable infection incidence, λ, between 0.01, 0.05, and 0.1. Fig. 1 presents the simulation results for this exercise.

Simulation Results.

Fig. 1a illustrates that the optimal cumulative lockdown rate increases with a lower infection incidence level. This rate was around 6 percent for an incidence level of 0.1, 9 percent for an incidence level of 0.05, and 12 percent for an incidence level of 0.01. What emerges from these numbers is that the relationship between the tolerable incidence level and the cumulative lockdown rate is not linear. As the tolerable infection incidence level decreases, the fraction of the population sent into lockdown increases, with the absolute value of this increase being smaller than the absolute value of the decrease. The optimal lockdown policy resulting from a given tolerable infection incidence level translates into corresponding dynamics for infection, death and economic cost. In particular, Fig. 1b shows that a lower tolerable incidence level results in

[11] In our empirical analysis, discussed in Section 5, the network of nursing homes in each U.S. state is not necessarily binary. Instead, A_{ij} ranges from 1 to 832 contacts, where i and j represent two distinct nursing homes. Since our empirical findings appear to be consistent with the simulation results, we believe that the binary nature of the network structure does not affect the qualitative dimension of our findings. In the planning problem, we choose values for the parameters of the production function that do not match those obtained from our data, for the purpose of illustration. Thus, one should interpret the quantitative outcomes of our model with caution. Nevertheless, in our empirical application, discussed in Section 5, we choose these parameters to match our U.S. state level data as closely as possible.

lower infection and death rates (see Fig. 1b and Fig. 1d). Fig. 1c illustrates the tradeoff between population health and economic well-being. A lower tolerable infection incidence level increases the economic cost of the pandemic. Indeed, if the tolerable infection incidence level is low, more individuals must be sent into lockdown, which decreases individuals' productiveness in the economy; this in turn produces a significant loss in terms of economic surplus. For instance, when the tolerable incidence decreases from 0.1 to 0.05, the fraction of the economic surplus lost to the pandemic increases from around 3 percent to over 5 percent; and a further decrease of the tolerable incidence level to 0.01 induces an economic surplus loss of around 6 percent. It follows that maintaining a lower infection incidence threshold is achieved at the expense of short-term economic prosperity.

"Please locate Fig. 1 here."

Robustness.

In Appendix G, we replicate the simulation results in Fig. 1 for scale-free, random, and lattice networks, in Figs. G1, G2, and G3, respectively. We also replicate Fig. 1 using recent epidemiological data on the COVID-19 Delta variant (see Fig. G4 in Appendix G). We find that all these additional simulation results are qualitatively consistent with the lockdown, disease, and economic costs dynamics described in Fig. 1.

4.2 The Role of Network Configuration

In Section 4.2, we fix the tolerable infection incidence λ to 0.01, and we vary the structure of network configuration, A, in the planning problem. For the sake of concreteness, we contrast four *idealized* network configurations (Keeling & Eames, 2005), namely a *lattice network* (Fig. 2a), a *small-world network* (Fig. 2b), a *random network* (Fig. 2c), and a *scale-free network* (Fig. 2d). These network types are some of the most frequently used to model disease transmission (see, e.g., Keeling and Eames (2005) and the references therein for a review of these networks). According to Keeling and Eames, "Each of these idealized networks can be defined in terms of how individuals are distributed in space (which may be geographical or social) and how connections are formed, thereby simplifying and making explicit the many and complex processes involved in network formation within real populations" (Keeling & Eames, 2005, p. 299). Following this viewpoint, the networks in Fig. 2 represent four societies, each of which contains 1000 agents. These societies are assumed to be identical in all ways except the configuration of their contact network. The four network configurations differ in their clustering of connections and their path lengths between nodes, two essential factors in disease spread.

"Please locate Fig. 2 here."

Simulation results.

We represent the simulation results in these idealized networks in Fig. 3. From Fig. 3, we observe that both the epidemic dynamics and the economic

costs of the disease are similar in the random network and small-world network structures. We can explain this similarity by the fact that short path lengths characterize both small-world and random networks. We illustrate the respective optimal lockdown policies in Fig. 3a for these four societies. The cumulative proportion of the population sent into lockdown peaks and flattens much earlier in the scale-free network society than in the lattice and small-world networks. At the onset of the pandemic, the lockdown is slightly stricter in the scale-free network compared to the lattice network. However, lockdown is always higher in random and small-world network configurations compared to lattice and scale-free configurations. The lockdown dynamics described in Fig. 3a respond to the disease dynamics that we illustrate in Fig. 3b for infection, and Fig. 3d for death. We observe that the reduction in initial growth in infection is more substantial in lattice networks compared with other networks. This is because a high spatial clustering of connections drives a more rapid saturation of local environment (Keeling & Eames, 2005). In addition, findings from theoretical models of disease spread through scale-free-networks indicate that infection is generally concentrated amongst agents with the highest number of connections (Chang et al., 2021; Newman, 2002; Pastor-Satorras & Vespignani, 2001). Therefore, sending these potential super-spreaders into lockdown can significantly reduce the spread of contagion. Our optimal lockdown policy is consistent with these findings since our simulation results suggest that placing highly connected hubs or agents in lockdown can significantly reduce spread in a scale-free network. Once they are in lockdown, the speed of infection from one individual to another is reduced (a simple example is a situation in which agents are connected through a star network). The situation is different in the small-world and random network societies, where short path lengths suggest a rapid spatial spread of disease. In these network structures, containing the contagion below a chosen infection incidence level requires more severe lockdown measures than in the scale-free network. As the epidemic continues, the dynamics of surplus loss that we represent in Fig. 3c, due to the pandemic, are also different across the four networks, with random and small-world networks suffering the most severe economic costs, as a result of severe lockdowns. The lowest lockdown in scale-free network (Fig. 3a) results in more infection and deaths in the long run (Fig. 3d).[12]

"Please locate Fig. 3 here."

Robustness with network density.

Following the comparative statics analyses on network topology described in Fig. 3, one might be interested in knowing how *network density* could affect the optimal lockdown policy, and therefore, the disease dynamics. To answer this question, we consider a society, A_k, consisting of $n = 1000$ agents connected through a small-world network (Watts & Strogatz, 1998) with $k \times n$ edges, where k represents the average number of connections per agent in the society.

[12]Based on the simulation results (Fig. G4 in Appendix G) that we obtain by replicating Fig. 1 with the COVID-19 Delta variant information, we conjecture that a similar exercise with the lattice, random, and scale-free network structures would yield consistent results.

The density $d(A_k)$ of the network A_k measures how many ties between agents exist compared to how many ties between agents are possible, given the number of nodes, n, and the number of edges, $k \times n$. Since A_k is an undirected network, $d(A_k) = \frac{2k}{n-1}$, and the network becomes more *dense* as k increases (i.e., there is an increase in the number of connections between agents). Fig. 4 represents the simulation results in society A_k, when $k \in \{2, 3, 4, 5\}$. The optimal lockdown dynamics displayed in Fig. 4a indicate that lockdown probabilities increase with network density. The social planner justifies this increase in lockdown probability by the fact that the infection rate is, as portrayed in Fig. 4b, higher in more dense societies at the onset of the pandemic. As the pandemic evolves, strict lockdown is effective in containing the infection so that, in the long run, less dense societies bear a higher number of deaths relative to more dense societies in Fig. 4c. Similarly to Fig. 3, stricter lockdowns result in fewer economic transactions and, as a result, more dense networks suffer a more significant loss in economic surplus. This phenomenon is displayed in Fig. 4c.

"Please locate Fig. 4 here."

Implications.

Our simple experiment in Section 4.2 highlights the fact that network configuration should be a key factor in designing optimal lockdown policies during a pandemic like COVID-19. These non-pharmaceutical policies have implications for both health dynamics and economic costs. Indeed, our illustrations are consistent with other studies showing that network configuration plays an essential role in the spread of infection and diffusion of information (e.g., Keeling and Eames (2005), Pongou and Serrano (2013, 2016), and recently, Kuchler et al. (2021), and Chang et al. (2021)). The numerical analysis also suggests that the wide range of variation in COVID-19 outcomes observed across countries, and across communities within countries, could be explained by differences in their network configuration. Several studies analyze the differences in COVID-19 outcomes between countries worldwide and communities within countries or regions. For comparisons among countries, see, e.g., Balmford, Annan, Hargreaves, Altoè, and Bateman (2020), and Sorci, Faivre, and Morand (2020); and for cross-community comparisons in COVID-19 outcomes in the United States, see, e.g., Chang et al. (2021), and Hong, Bonczak, Gupta, Thorpe, and Kontokosta (2021).

4.3 Network Centrality and Optimally Targeted Lockdown

Our third comparative statics analysis highlights how lockdown policies can be optimally targeted at individuals based on their characteristics. The specific individual characteristic we consider is an individual's centrality in their contact network. In general, certain agents occupy more central positions than others in the prevailing contact network of a networked economy (see, e.g., Chang et al. (2021)). This can be due to a variety of factors, including the distinct social and economic characteristics of each individual. It is argued

that individuals who occupy more central positions in networks are more likely to be infected and to spread an infection, e.g., Anderson and May (1992), Pastor-Satorras and Vespignani (2001), Newman (2002), Hethcote and Yorke (2014), Pongou and Tondji (2018), and Rodrigues (2019). This suggests that an optimal lockdown policy should be targeted at more central agents in a network. However, various measures of network centrality exist, and it is not clear which of these measures is most predictive in the context of a pandemic like COVID-19.

To address this issue, we consider four popular network metrics: degree centrality, eigenvector centrality, betweenness centrality, and closeness centrality. For clarity, we will briefly define each of these four measures of network centrality in Appendix E. To answer how each of the aforementioned network metrics predicts the probability of lockdown, we consider a society in which agents are connected through a small-world network with $2 \times n$ edges. Agents occupy distinct positions in this network, resulting in some agents being more central than others. For robustness, our simulation analysis assumes three different values for the tolerable infection incidence λ: 0.01, 0.05, and 0.1.

Simulation Results.

Table 1 reports the correlation between each of our network metrics and the average optimal lockdown probabilities for different values of the tolerable infection incidence, λ, in a small-world network. Our simulation results in Table 1 suggest that the four centrality measures positively correlate to the likelihood of lockdown under the optimal lockdown policy. This correlation is statistically significant, as implied by the different p-value statistics. Moreover, the predictive force of lockdown obtained for each measure of centrality increases with larger values of λ.

"Please locate Table 1 here."

Robustness.

In Table G2 in Appendix G, we provide robustness checks for other correlations between the four network metrics and average optimal lockdown probabilities in the lattice, random, and scale-free networks. We observe that all other centrality measures are positively correlated with the average optimal lockdown probabilities, apart from the lattice network. Also, in line with the small-world network, the degree centrality appears to have a stronger correlation with the lockdown in the random and scale-free networks. Though the correlation between the network metrics and optimal lockdown probabilities becomes stronger as the tolerable infection incidence increases in small-world and scale-free networks, the direction of the changes is non-monotonic in lattice and random networks. The latter simulation results suggest that we should be cautious about making any conclusions about the sign and direction of the relationship between the tolerable infection incidence, λ, the network centrality measures, and the optimal lockdown probabilities. Nevertheless, the simulation results in Table 1 and in Appendix G (Tables G2 and G3) imply that in a

society organized as either a small-world network or a scale-free network, with a higher level of tolerance for the virus, more central individuals will suffer fewer deaths as a result of being more severely isolated. In Section 5, we use data from the network of U.S. nursing and long-term care homes (M.K. Chen et al., 2021) to test some of these simulation results.

Remark.

Intuitively, though a full lockdown may be a solution in a pure epidemiological model, it cannot be optimal in our N-SIRD model because the goal is to disconnect the contact network while maintaining economic activities. It follows that under our optimal lockdown policy, not all agents would be in the lockdown. This analysis highlights the limitations of quasi-universal lockdown policies such as those implemented in several countries worldwide in the early period of COVID-19. Our policy recommendations are consistent with studies and reports suggesting shutting down only particular sectors of society during a pandemic like COVID-19 (see, e.g., Acemoglu et al. (2021), Bosi et al. (2021), Chang et al. (2021), and Pestieau and Ponthière (2022)). Specifically, lockdowns should target, sectors that serve as social and economic hubs and attract large numbers of individuals, such as large shopping centers, airports and other public transportation infrastructures, schools, certain government buildings, entertainment fields, parks, and beaches, among others.

5 Empirical Application

In this section, we calibrate our N-SIRD model, estimate the tolerable COVID-19 infection incidence level for 26 U.S. states, and test some of our model's predictions using unique data on networks of the U.S. nursing homes and long-term care facilities.

Relevance.

The example of U.S. nursing home networks is a relevant test of our theoretical model for two main reasons. First, the senior population (adults 65 and older) accounts for a significant share of COVID-19 deaths in the U.S. As of September 24, 2021, seniors account for 16% of the U.S. population but 77.9% of U.S. COVID-19 deaths (Yang, 2021). Nursing and long-term care facilities have been at the center of many COVID-19 outbreaks, and this situation led the U.S. federal government to ban nursing home visits on March 13, 2020. This restriction has enabled researchers from the "Protect Nursing Homes" project to construct a network of physical contacts in U.S. nursing homes, using geolocation data for 50 million smartphones. They observed that 5.1% of smartphone users (approximately 501,503 staff and contractors) who visited a nursing home for at least 1 hour also visited another facility during the 11-week study period, even after visitor restrictions were imposed. The ban on nursing home visits—an example of a lockdown policy to reduce contagion in nursing homes—created an environment where the network of contacts was

the primary source of virus spread. Second, as we explain in Section 4, the calibration of production functions for senior care services in each U.S. state can be viewed as a representation of a simple production environment in the optimal control problem of our theoretical model.

Capturing the tradeoff between saving lives and economic prosperity.

The main exogenous constraint introduced in the theoretical model, the tolerable infection incidence level λ, reveals the extent to which governors in different U.S. states are willing to curb the spread of SARSCOV-2, the virus that causes COVID-19. In order words, λ captures the governor's tradeoff between health and wealth. A high value for λ is equivalent to a "laissez-faire" policy, indicating a planner's inclination to maximize economic gains even if this theoretically results in more infections and deaths. Section 5.1 estimates the values of λ for 26 U.S. states. Furthermore, since COVID-19 responses have been highly politicized in the U.S. and given the large heterogeneity in the values of λ, we investigate how political ideology (measured by the party of the governor) and other state specific factors determine λ.[13] Section 5.2 uses the estimated values of λ to test some theoretical predictions of our N-SIRD model with lockdown. Precisely, we explore whether the simulation results are consistent with reality. For instance, we examine whether "laissez-faire" policies lead to more deaths. We also investigate the effect of network centrality and the tolerable infection incidence on COVID-19 death in nursing facilities.

5.1 Estimation of COVID-19 Tolerable Infection Incidence

5.1.1 Data, Calibration, and Estimation

To calibrate our parameter of interest, we use data from several sources. Data on the economic variables come from the Bureau of Labor Statistics and the Senior Living project.[14]. Data on the U.S. nursing home networks were obtained from M.K. Chen et al. (2021). We obtain the calibration of the epidemiological parameters from Statista.[15] Using the data on U.S. nursing home networks, we calibrate a nursing home's production function; for more details on this calibration, we refer to Section F.1 in Appendix F. We describe in

[13] Neelon et al. (2021) suggest that there is an association between a governor's party affiliation and COVID-19 infections and deaths (also, see, e.g., Baccini, Brodeur, and Weymouth (2021), and H.-F. Chen and Karim (2021) for additional evidence linking political party of leaders and COVID-19 fatalities). We complement these findings by investigating the association between the COVID-19 estimated tolerable infection incidence and the governor's party affiliation. More importantly, we view our analysis as an "external" validation of our estimation of λ; indeed, it follows from the aforementioned studies that λ should be higher for states governed by Republicans than for states governed by Democrats.

[14] We gathered information from the Senior Living project on 9/9/2021 at https://www.seniorliving.org/nursing-homes/costs/.

[15] This data is available at https://www.statista.com. Statista provides information on the reproduction number for COVID-19, and the COVID-19 infection and death rates among nursing home residents in each U.S. state as of September 2020.

Table 2, all sources of calibrated and estimated parameters for each U.S. state, which we use in our empirical application.

"Please locate Table 2 here."

U.S. nursing home networks.

We consider each nursing home as a node in the transmission network. Two nursing homes are connected if the same smartphone signal is recorded in both homes' locations. The number of distinct signals recorded gives a weight to the connection or link between two nursing homes. Nursing and long-term care facilities display a wide range of connectedness with other facilities. M.K. Chen et al. (2021) use different network metrics to predict COVID-19 in nursing homes. In this empirical application of our N-SIRD model, we focus on the eigenvector centrality, which measures the extent to which a nursing home in a U.S. state is connected to other highly connected nursing homes in the state.[16] To illustrate how the eigenvector centrality measure differs across nursing homes, we present network graphs for a subset of homes in six states as depicted in Fig. 5 and summarized in Table 3. More-connected nursing facilities are generally toward the center of each graph, and facilities with fewer contacts are on the periphery. Table 4 summarizes the descriptive statistics of U.S. nursing homes. We refer to M.K. Chen et al. (2021) for additional details on nursing homes characteristics and network centrality measures in these care facilities.

"Please locate Fig. 5 here."

"Please locate Tables 3 and 4 here."

Estimation of λ.

We estimate the parameter measuring the governor's tolerable infection incidence using a simulated minimum distance estimator (Forneron & Ng, 2018; Gertler & Waldman, 1992). Indeed, for each potential value of λ, the planner's problem is solved and the dynamics of death in the model over 77 days is compared to raw data on elderly death dynamics provided by the New York Times death count from May 31 to August 16, 2020. The value of λ that will minimize the distance between the two dynamics will be the estimate of the tolerable infection incidence level for that U.S. state's governor. In Section F.2 in Appendix F, we provide additional explanation on estimating λ. The procedure is carried out for 26 U.S. states and the estimate values of λ are displayed in Fig. 6. For each of the 26 U.S. states, the tolerable infection incidence level λ is significantly different from zero. The estimated tolerable infection incidence levels range from 0.0006 for the state of Missouri (MO) to 0.45 for Alabama (AL). The average value of λ is 0.12 and the standard deviation is 0.13 indicating a substantial level of dispersion. We investigate in Section 5.1.2, the possible sources of such heterogeneity.

"Please locate Fig. 6 here."

[16] Table G4 in Appendix G shows that our main empirical results are robust when replacing eigenvector centrality by the degree centrality.

5.1.2 Origins of the Tolerable Infection Incidence Heterogeneity

Whether it is about economic lockdowns, mask mandates, or COVID-19 vaccines, the public debates in the U.S. have been divided along political lines (Adolph, Amano, Bang-Jensen, Fullman, & Wilkerson, 2021; Neelon et al., 2021). The extent to which this division has affected the COVID-19 pandemic is at the heart of a new and growing literature. We contribute to this literature by examining whether the party affiliation of a U.S. state's governor predicts the tolerable COVID-19 infection incidence. We regress the tolerable infection incidence level on the party affiliation of the state governor in the period covered by the sample (May 31 to August 16, 2020) and other controls. This regression sheds light on the most critical determinants of the U.S. state's choice of the tolerable COVID-19 infection incidence level. The analysis also represents an attempt to validate our estimation of the parameter λ using information from external sources.

Regression results.

The estimation results shown in Table 5 indicate that Democratic governors have a tolerable infection incidence that is 8% lower than that of their Republican counterparts. Thus, Republican governors are more inclined to implement "laissez-faire" policies, which mirrors the traditional pro-market position of the party. This statement is in line with Baccini and Brodeur (2021), who find consistent results on the role of political ideology in the response of U.S. states to the COVID-19 pandemic. For instance, their results suggest that during the early COVID-19 epidemic, Democratic governors emphasized health and safety and were significantly more likely to implement a statewide stay-at-home order. By contrast, Republican governors were particularly concerned about the economic costs of stay-at-home measures and were less likely to implement those policies. Unsurprisingly, we find there is a positive association between the number of deaths in a U.S. state's nursing homes and tolerable COVID-19 infection incidence level in that state. However, having a higher number of deaths in nursing homes seems to reduce the gap in the tolerable infection incidence between Republican and Democratic governors, as illustrated by estimates in Columns (2) to (4) of Table 5. Governors from different parties therefore tend to converge in their policies when faced with a high death count. The estimation results also suggest that the gender of the governor has an effect on the tolerable infection incidence level, with this level being higher in female governors by about 7%. Moreover, being located in the South increases the tolerable infection incidence level by 5%.

"Please locate Table 5 here."

In summary, our analysis suggests that both the ideological orientation of a state's governor and the statewide severity of the pandemic impact the choice of the tolerable COVID-19 infection incidence across the 26 U.S. states sampled. Additionally, we find the gender of a U.S. state's governor, as well as

a state's geographic location as essential determinants of tolerable COVID-19 infection incidence level.

5.2 Testing Some N-SIRD Model's Predictions

In our empirical analysis, we estimate the following linear model:

$$\begin{aligned} covid\_death_{ijs} &= a_0\lambda_s + a_1 Eig\_Cent_{ijs} + a_2 County\_ssa_{js} + a_3 D\_Profit_{ijs} \\ &+ b_1\lambda_s \times Eig\_Cent_{ijs} + b_2\lambda_s \times County\_ssa_{js} + b_3\lambda_s \times D\_Profit_{ijs} \\ &+ c' X_{ijs} + \theta_j + \varepsilon_{ijs}, \end{aligned} \tag{5}$$

where $covid\_death_{ijs}$ is a variable counting the total number of COVID-19 deaths in nursing home i, in County j and U.S. state s; λ_s is the tolerable infection incidence in U.S. state s; Eig_Cent_{ijs} is the eigenvector centrality index for the nursing home; $County\_ssa_{js}$ is the county j's average socio-economic status; D_Profit_{ijs} is an indicator for whether nursing home i is for profit (1 if for-profit, and 0 otherwise); X_{ijs} represents other exogenous characteristics of the nursing home including the constant; and θ_j is the county fixed effect.[17] The parameters of interest are a_0, a_1, a_2, a_3, b_1, b_2, and b_3. The estimated values of these parameters can be found in Table 6. Estimating the tolerable infection incidence level in each U.S. state allows us to verify some of the model's predictions.

"Please locate Table 6 here."

Tolerable infection incidence and COVID-19 death.

Fig. 1d in Section 4.1 illustrates the relationship between the tolerable infection incidence level and the death dynamics. This statics comparative analysis implies that a more higher value for λ is associated with more COVID-19 deaths. The OLS estimation results in Table 6 suggest that there is a positive association between the tolerable infection incidence level and the total number of COVID-19 deaths in a nursing home. A five standard-deviation increase in the tolerable infection incidence is expected to lead approximately to one additional death in a nursing home everything else being equal. This means that laissez-faire policies will result in more COVID-19 deaths. This result remains robust after controlling for county fixed-effects, the level of income of a nursing home's residents (as proxied by the average socio-economic status in the county), the quality of care provided, and whether the nursing home operates on a for-profit basis.

[17] The choice of the total number of COVID-19 deaths rather than cases, as the outcome variable, is motivated by two reasons. First, the number of COVID-19 cases contains both asymptomatic patients and those who will later recover, so it cannot be an appropriate measure of the human cost of the pandemic. Second, as represented in Fig. 1b, depending on the point in time during the pandemic, there may be no difference in the number of infected individuals as a function of the tolerable infection incidence. On the contrary, the total number of deaths displays unambiguous dynamics which makes the theoretical predictions of our N-SIRD model easier to test. In addition, the total number of deaths is unambiguously a proxy for the human cost of the pandemic.

Tolerable infection incidence, network centrality, and COVID-19 death.

The simulation results uncovered in Section 4 suggest that the level of network centrality plays a pivotal role in the choice of optimal lockdown and the diffusion of an epidemic that spread through networks. The optimal lockdown policy targets more central individuals with a higher probability. Table 1 in Section 4.3 suggests that higher values of tolerable infection incidence levels are associated with a higher likelihood of lockdown for central agents in a network. Therefore, our simulation would predict that adopting a laissez-faire approach (i.e., increase in λ) will reduce the impact of network centrality on the number of COVID-19 deaths because more central individuals are likely to be sent into lockdown. In other words, under a laissez-faire policy, the difference in the number of deaths between central and peripheral nursing homes is reduced. The regression results in Table 6 validate this prediction. Column (1) shows that being more central is associated with more COVID-19 deaths in the nursing homes. Column (2) shows the interaction between eigenvector centrality and the tolerable infection incidence. The interaction term has a negative and statistically significant effect on total COVID-19 deaths. An increase in the level of the tolerable infection incidence therefore reduces the relative death toll of more central nursing homes. Columns (2) and (5) of Table 6 show the robustness of this result to the introduction of several controls. We also verify another prediction of our model's simulation in the sample under investigation. Our results complement M.K. Chen et al. (2021) by showing that, while the level of eigenvector centrality matters in the propagation of the epidemic and death count, there exists heterogeneity in the extent of its relevance. More precisely, we show that the social planner's tolerable infection incidence affects the relationship between the level of centrality and the number of COVID-19 deaths. This relationship is less pronounced under a laissez-faire regime.

Tolerable infection incidence and wealth accumulation.

The simulations in Section 4 also show the relationship between the tolerable incidence and economic performance. Fig. 1c suggests that more laissez-faire policies are associated with a lower total economic cost. The estimation results in Table 8 put this prediction to a test by estimating the effect of U.S. states' tolerable COVID-19 infection incidence on their level of GDP growth in 2020. We present in Table 7, the descriptive statistics of GDP and U.S. states' governorship political affiliation and gender in 2020. In accordance with the theoretical simulations, our estimation results suggest a positive relationship between λ and the GDP growth. The effect of the tolerable infection incidence on economic growth is larger for republican governors. These results are robust to the inclusion of controls for regional differences and the gender of the governor.

"Please locate Tables 7 and 8 here."

Additional regression results.

We also assess how laissez-faire policies affect the relationship between the COVID-19 death toll, economic conditions, and type of nursing home (for-profit or not). Column (5) in Table 6 shows that laissez-faire policies more negatively affect nursing homes in economically deprived counties. Our analysis also shows that for-profit nursing homes have 27% more deaths compared to not-for-profit nursing homes (see Columns (1) to (3) in Table 6). Moreover, the type of the nursing home and the tolerable infection incidence are the main drivers of the difference in COVID-19 deaths in nursing homes. Indeed, when we introduce the interaction term between λ and for-profit (D_Profit) in Column (4), both the effects of λ and the for-profit indicator (D_Profit) become smaller in absolute value and statistically insignificant; only the interaction term has a positive and statistically significant coefficient, meaning that the detrimental effects of laissez-faire policies are primarily present in nursing homes that operate on a for-profit basis. We also note that better rated nursing homes have significantly less deaths.

Summary.

The findings of Table 8 validate some essential predictions of the N-SIRD model using data from nursing home networks in 26 U.S. states. Indeed, we provide evidence suggesting that a higher tolerable infection incidence is associated with more COVID-19 deaths. Moreover, centrality plays an essential role in optimal lockdown, and laissez-faire policies significantly interact with network centrality. We also show that the tolerable infection incidence seems to mediate the impact of economic variables on the human cost of the pandemic. The existence of a positive correlation between the tolerable infection incidence and economic performance is tested and validated in our sample.

6 Concluding Remarks

This study addresses the problem of finding an optimal lockdown policy during a pandemic for a social planner who *prioritizes* health over short-term economic gains. Agents are connected through a weighted network of contacts, and the planner's objective is to determine the policy that contains the spread of infection below a *tolerable* incidence level and maximizes the present discounted value of real income, in that order of priority. We formalize this tradeoff by using lockdown as a policy instrument in an optimal control problem that mixes an individual mean-field epidemiological model and a simple production environment.

Our analysis reveals that the planner's optimal lockdown policy depends on tolerable infection incidence level and social network structure. Using simulation-based comparative statics analyses in combination with early COVID-19 data, the paper highlights the crucial role of network structure in infection spread. Mainly, it quantifies the tradeoff between the tolerable infection incidence and human losses on the one hand and the economic losses due

to the pandemic on the other hand. The simulation exercises also show how different network centrality measures correlate with individual lockdown probabilities and how this correlation varies with the tolerable infection incidence level.

We use unique data on U.S. nursing home networks, as well as other data sources, to calibrate our model and estimate the tolerable COVID-19 infection incidence level (λ) for 26 U.S. states. Our estimates show significant variation in λ across U.S. states. This variation is partly explained by COVID-19 fatalities, the gender of a state's governor, the party affiliation of a state's governor, and states' geographic location. Using these estimated values of λ, we find that policies that tolerate more virus spread (laissez-faire) are associated with an increased number of deaths in nursing homes and an increase in a state's GDP growth. We also find significant interactions between λ and other essential variables. In particular, we find that laissez-faire policies are more harmful to nursing homes that are more peripheral in networks. Additionally, laissez-faire policies are also more detrimental to nursing homes in deprived counties and those operating on a for-profit basis. These latter findings are relevant and valid for organizations that seek to maximize economic gains.

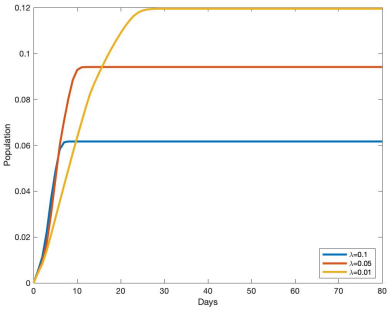

(a) Dynamics of Lockdown

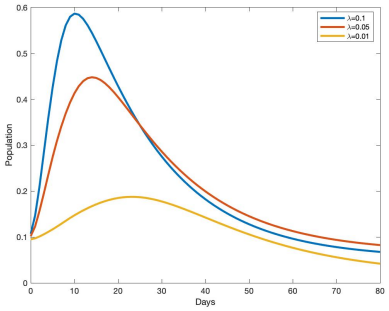

(b) Dynamics of Infection

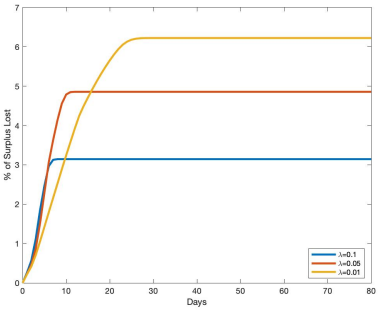

(c) Dynamics of Economic Cost

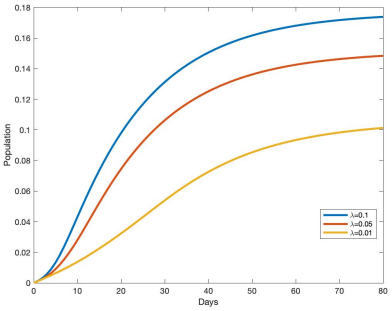

(d) Dynamics of Death

Fig. 1: Health versus wealth tradeoff in a small-world network. Notes: We perform three sets of simulations with three different values of the tolerable infection incidence λ: 0.01, 0.05, and 0.1. The results are displayed in a two-dimensional graphic, with days on the horizontal axis, and the percentage of population affected for the variable (infection, lockdown, or death) on the vertical axis. In each period, a point in the graphic represents the average value of individual probabilities. For the economic cost, the vertical axis represents the percentage of economic surplus lost relative to the economy without the pandemic. Each graph shows three curves corresponding to three dynamics for a single variable of interest and a given value of λ. All variability within each curve in each graph is a result of the stochastic nature of transmission and not variation in the network or λ.

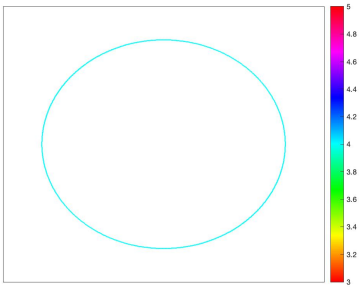

(a) Lattices Network

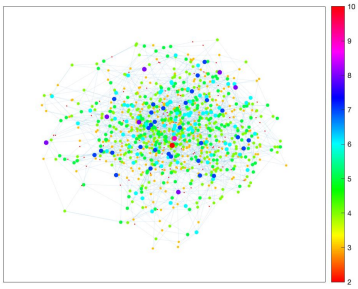

(b) Small-World Network

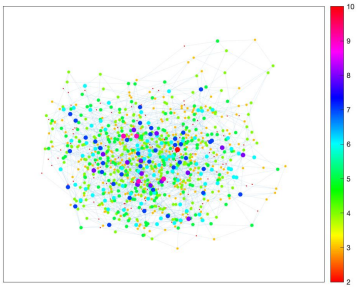

(c) Random Network

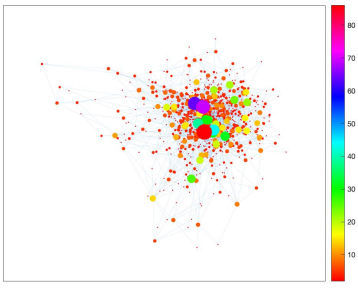

(d) Scale-Free Network

Fig. 2: Simple network structures. Notes: Four distinct network types containing 1000 agents. Random networks display homogeneity of agent-level network properties and low clustering. Lattices are homogeneous at the agent level, and they show high clustering. Lattice networks also exhibit long path lengths, i.e., it takes many steps to move between two randomly selected agents, whereas random networks have short path lengths. Small-world networks display high clustering and short path lengths. Scale-free networks capture different levels of heterogeneity (for example, super-spreaders) in populations. In all four graphs, the average number of contacts per agent is 2. In each network, we represent agents with high contacts by larger dots, and we shade each node according to its number of direct contacts using the scale beside each graph.

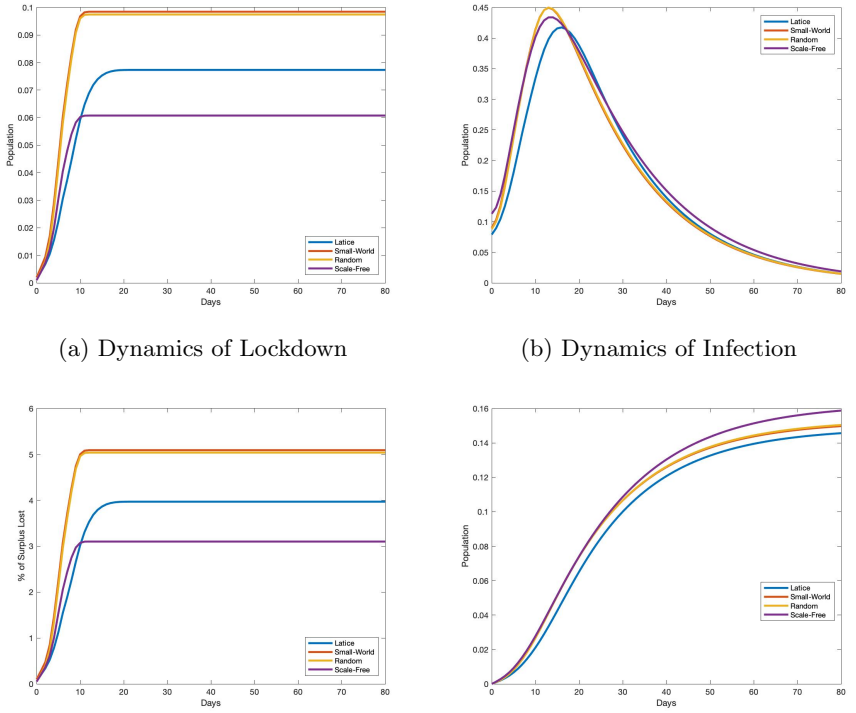

(a) Dynamics of Lockdown

(b) Dynamics of Infection

(c) Dynamics of Economic Cost

(d) Dynamics of Death

Fig. 3: Optimal disease and economic cost dynamics in networks. Notes: N-SIRD epidemic process, lockdown, and economic cost dynamics on the four network types shown in Fig. 2. Each graph shows four curves corresponding to four networks for a single variable of interest. All variability within each curve in each graph is a result of the stochastic nature of transmission and not variation in the network. In the simulation, we assume that the tolerable infection incidence $\lambda = 0.01$. The results are displayed in a two-dimensional graphic, with days in the horizontal axis, and the percentage of population affected for the variable (infection, lockdown, or death) illustrated on the vertical axis. In each day, a point in the graphic represents the average value of individual probabilities. For the economic cost, the vertical axis represents the percentage of economic (or surplus) loss relative to the economy without the pandemic. Based on the simulation results (Fig. G4 in Appendix G) that we obtain by replicating Fig. 1 with the COVID-19 Delta variant in the small-world network, we conjecture that a replication of Fig. 3 would yield qualitatively consistent results.

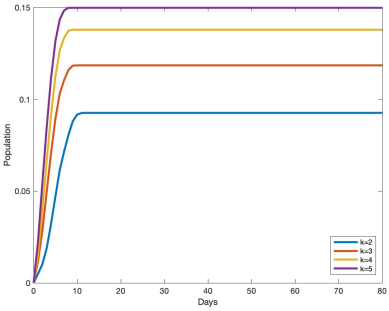

(a) Dynamics of Lockdown

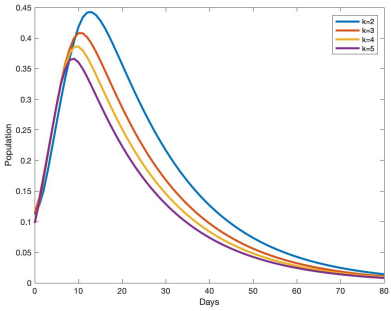

(b) Dynamics of Infection

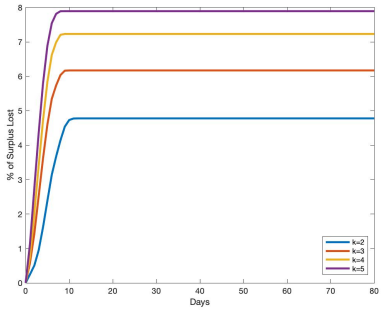

(c) Dynamics of Economic Cost

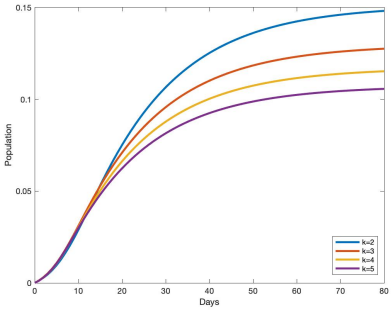

(d) Dynamics of Death

Fig. 4: Optimal disease and cost dynamics in a small-world network with different densities. Notes: In our simulations, we assume that $\lambda = 0.01$. The results are displayed in a two-dimensional graphic, with days in the horizontal axis, and the percentage of population affected for the variable (infection, lockdown, or death) illustrated on the vertical axis. In each period, a point in the graphic represents the average value of individual probabilities. For the economic cost, the vertical axis represents the percentage of economic surplus lost relative to the economy without the pandemic. The density of network A_k is $d(A_k) = \frac{2k}{n-1}$, where the parameter k represents the average number of connections per agent in network A_k, and n number of nodes. Based on the simulation results (Fig. G4 in Appendix G) that we obtain by replicating Fig. 1 with the COVID-19 Delta variant in the small-world network, we conjecture that a replication of Fig. 4 would yield qualitatively consistent results.

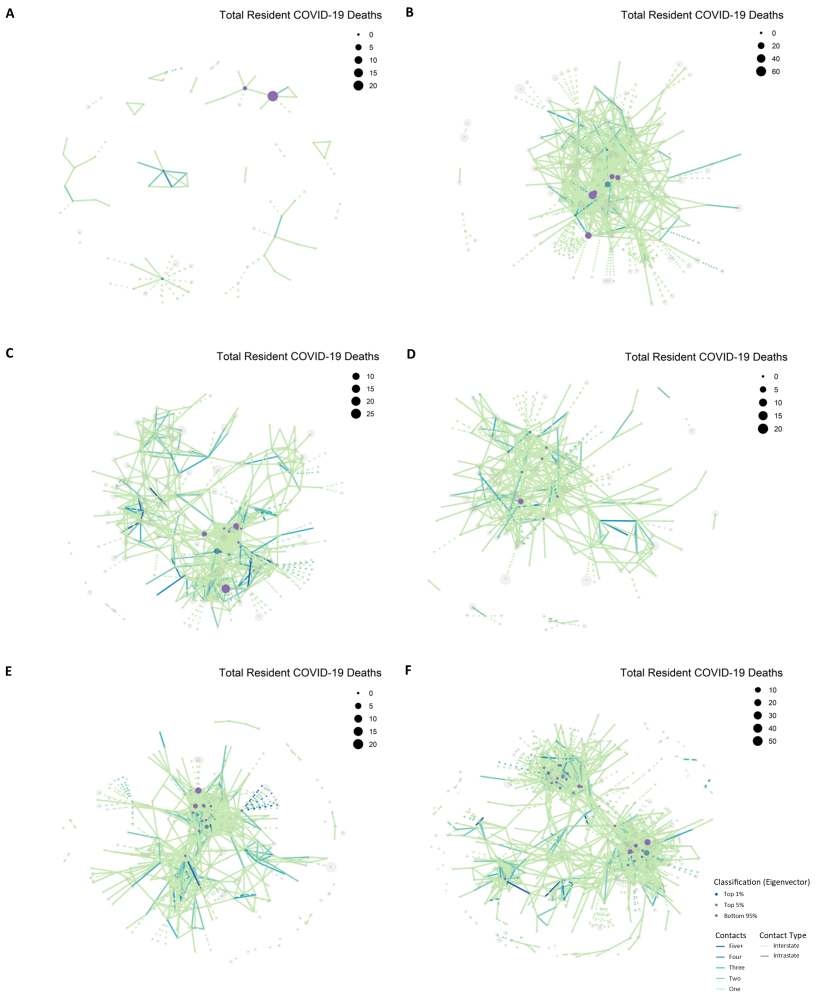

Fig. 5: Nursing home network structures in South Dakota (A), Connecticut (B), Louisiana (C), Colorado (D), Oklahoma (E), and Missouri (F). Notes: Details for each network configuration are provided in Table 3. In the network, node size varies with the number of COVID-19 deaths among residents reported to the U.S. Centers for Medicare & Medicaid Services as of May 31, 2020; edge colour differs with the number of contacts between nursing homes; a solid (resp. dotted) edge line corresponds to a connection between two nursing homes within the same U.S. state (resp. in two different states); and node colour differences are based on eigenvector ranking, with the dark red colour, for example, highlighting the top 1% of facilities with high eigenvector centrality in the network.

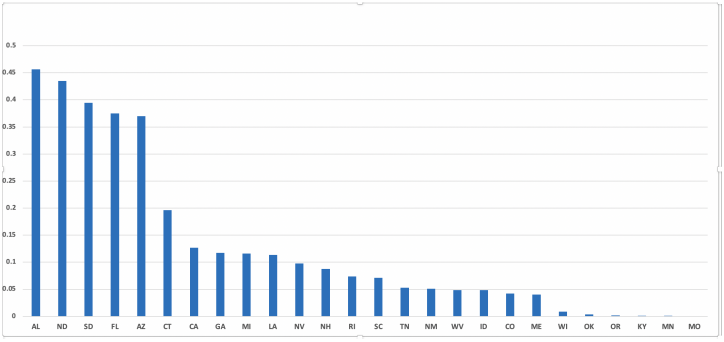

Fig. 6: U.S. state's tolerable COVID-19 infection incidence level λ. Notes: The parameter λ estimates the tolerable COVID-19 infection incidence of the U.S. state governor from May 31 to August 16, 2020. Using the data and the N-SIRD model with lockdown, we estimate λ for 26 U.S. states. The estimates range from 0.0006 for Missouri (MO) to 0.45 for Alabama (AL). The average value of estimates is 0.12 and the standard deviation is 0.13.

Table 1: Network centrality and lockdown probability in a small-world network

λ	Degree		Closeness		Betweness		Eigenvector	
	corr	p-value	corr	p-value	corr	p-value	corr	p-value
0.1	**0.36**	8e-33	**0.34**	9e-29	**0.33**	3e-27	**0.29**	1e-20
0.05	**0.25**	5e-16	**0.21**	1e-11	**0.21**	6e-12	**0.17**	1e-07
0.01	**0.26**	1e-16	**0.18**	4e-09	**0.18**	3e-09	**0.13**	4e-05

Note: Table 1 illustrates the correlation (corr) between measures of centrality and average optimal lockdown probability in a small-world network for three values of λ. The p-value for each centrality measure is for the test of the hypothesis H_0 $\rho = 0$ vs H_1 $\rho \neq 0$. In Table G2 in Appendix G, we replicate Table 1 for scale-free, random, and lattice networks. We also replicate Table 1 using recent epidemiological data of the COVID-19 Delta variant (see Table G3 in Appendix G). We find that the simulation results in Table G2 are qualitatively consistent with the findings in Table 1. We conjecture that a similar replication of Table G2 with updated COVID-19 information in lattice, random, and scale-free network would yield consistent qualitative results as in Table G3.

Table 2: Description and sources of calibrated and estimated parameters for each U.S. state

Parameters or Variables	Value	Definitions and Sources	Utilization
Epidemiological			
β	$R_0/18$	The COVID-19 reproduction numbers R_0 estimated during April to July 2020, from Statista	Calibration
γ	(1-death/case)/18	case and death per 1000 in nursing homes in each U.S. state as of Sep. 2020 from Statista	Calibration
κ	(death/case)/18	case and death per 1000 for in nursing homes in each U.S. state as of Sep. 2020 Statista	Calibration
Death Count	80% of COVID-19 death	New York Times in each U.S. state from May 31 to August 16, 2020	Calibration
A	Network of nursing homes	Protect Nursing Home Project	Calibration
Economic			
Price	Average hourly cost of a Private Room	Senior Living Project	Calibration
Wage	Average hourly wage by State	BLS Calibration	
α	Cobb-Douglass production function	Replication data from Chen et al. (2021) Estimation for each State	Calibration.
Regressions Table 4 and 5	variables	Replication data from M.K. Chen et al. (2021) and authors' calculation	Estimations
Regression Table 6	variables	Replication data from M.K. Chen et al. (2021) and authors' calculation	Estimations
Capital	Number of beds in the nursing home	Replication data from M.K. Chen et al. (2021)	Calibration

Table 3: Network characteristics for six selected U.S. nursing home networks

States	Number of nursing homes	COVID-19 deaths Max	Mean	Sd	Eigenvector Mean	Sd
South Dakota	103	22	0.22	2.17	0.043	0.17
Connecticut	196	67	7.31	10.46	0.13	0.21
Louisiana	259	26	2.68	5.06	0.09	0.22
Colorado	214	22	1.49	3.73	0.11	0.18
Oklahoma	257	17	0.3	1.59	0.08	0.18
Missouri	483	21	0.56	2.52	0.07	0.15

Note: Data comes from M.K. Chen et al. (2021). COVID-19 deaths are confirmed among residents reported to the U.S. Centers for Medicare and Medicaid Services (CMS) as of May 31, 2020. "Sd" means standard deviation.

Table 4: Descriptive statistics of U.S. nursing homes

Variable	Mean (standard deviation)
COVID-19 information	
Cases	84.47 (237)
Death	1.84 (5.94)
Network metrics	
Home degree centrality	6.21 (7.83)
Home eigenvector centrality	0.08 (0.18)
Regulatory measures	
For profit	0.703
Number of beds	105.61 (59.04)
Number of beds occupied	76.97 (48.01)
CMS quality rating (1-5)	3.69 (1.24)
County SSA	391.39 (273.53)
Number of nursing homes	15277

Note: Data are from M.K. Chen et al. (2021). Binary variables are percent of nursing homes; continuous variables are mean values, with standard deviations in parentheses.

Table 5: Origins of the tolerable COVID-19 infection incidence heterogeneity

	(1)	(2)	(3)	(4)
Republican Governor	0.0973***	0.104***	0.0999***	0.0756***
	(33.06)	(33.28)	(31.93)	(20.59)
Republican × Covid_Death		-0.00293***	-0.00376***	-0.00351***
		(-5.72)	(-7.12)	(-6.84)
Covid_Death		0.00280***	0.00291***	0.00289***
		(11.00)	(10.48)	(9.61)
Female Governor			0.0536***	0.0693***
			(11.15)	(14.17)
South				0.0514***
				(12.61)
Constant	0.174***	0.0718***	0.0656***	0.0553***
	(63.55)	(63.14)	(49.25)	(33.09)
Observations	6985	6564	6564	6564
R^2	0.128	0.138	0.158	0.183

Note: The dependent variable is the U.S. state's tolerable COVID-19 infection incidence (λ). Standard errors are robust to heteroscedasticity of unknown form. * $p < 0.1$, ** $p < 0.05$, *** $p < 0.01$, t statistics are in parentheses.

Table 6: Estimation of the effects of laissez-faire policies (λ) on number of deaths in U.S. nursing homes

	(1)	(2)	(3)	(4)	(5)
λ	0.713**	1.063***	2.127***	-0.105	1.573**
	(2.04)	(3.19)	(3.25)	(-0.21)	(2.12)
Eig_Cent	1.006***	1.482***	1.026***	1.011***	1.533***
	(3.27)	(3.98)	(3.35)	(3.29)	(4.11)
County_ssa	-0.000780	-0.000824	-0.000521	-0.000793	-0.000584
	(-1.09)	(-1.15)	(-0.72)	(-1.11)	(-0.81)
D_Profit	0.266**	0.268**	0.269**	0.101	0.0836
	(2.28)	(2.29)	(2.30)	(0.73)	(0.60)
$\lambda\times$ Eig_Cent		-3.944**			-4.157**
		(-1.97)			(-2.08)
$\lambda\times$ County_ssa			-0.00446**		-0.00445**
			(-2.47)		(-2.48)
$\lambda\times$ D_Profit				1.231**	1.387**
				(1.97)	(2.20)
Overall_Rating	-0.207***	-0.207***	-0.207***	-0.210***	-0.210***
	(-5.07)	(-5.07)	(-5.06)	(-5.13)	(-5.12)
County FE	Yes	Yes	Yes	Yes	Yes
Observations	6478	6478	6478	6478	6478
R^2	0.072	0.073	0.073	0.073	0.074

Note: Standard errors are robust to heteroscedasticity of unknown form. t statistics in parentheses. * $p < 0.1$, ** $p < 0.05$, *** $p < 0.01$. In Table G4, we show that our main empirical results in Table 6 are robust when replacing eigenvector centrality by the degree centrality.

Table 7: Descriptive statistics of GDP and U.S. state governorship political affiliation and gender in 2020

	Mean	Standard Deviation	Minimum	Maximum
GDP Growth, %	-3.46	1.47	-7.00	-0.10
Democrat Governor	0.47	0.50	0.00	1.00
Female Governor	0.18	0.39	0.00	1.00

Table 8: Estimation of the effects of laissez-faire policies on U.S. state's GDP growth in 2020

	(1)	(2)	(3)	(4)	(5)
λ	3.812**	4.290**	5.401**		
	(2.57)	(2.15)	(2.35)		
Democrat Governor		0.0554	0.845		-2.040**
		(0.08)	(1.02)		(-2.22)
Female Governor		-0.513	-0.765		-0.593
		(-0.91)	(-1.31)		(-0.96)
South		-1.083*	-1.124*		-1.261*
		(-1.78)	(-1.92)		(-2.06)
Democrat $\times$ λ			-10.15*		
			(-1.95)		
$log(\lambda)$				0.169	0.420**
				(1.47)	(2.25)
Democrat $\times$ $log(\lambda)$					-0.540**
					(-2.38)
Constant	-4.100***	-3.674***	-3.804***	-3.088***	-1.700*
	(-11.87)	(-5.16)	(-5.32)	(-6.57)	(-2.05)
Observations	26	26	26	26	26
R^2	0.165	0.307	0.382	0.057	0.320

Note: Standard errors are robust to heteroscedasticity of unknown form. * $p < 0.1$, ** $p < 0.05$, *** $p < 0.01$, t statistics are in parentheses.

Appendix A The final size of the pandemic

To reflect the impact of the epidemic in a totally susceptible population, we set $s_i(0) \approx 1$ and assume following Andreasen (2011) that $x_i(0)$ is positive with $x_i(0) \approx 0$ for all $i \in N$. We also follow Brauer (2008) by stating that $x_i(t) \to 0$ when $t \to \infty$, while there exists some real number $s_i(\infty)$ such that $s_i(t) \to s_i(\infty)$ when $t \to \infty$. The first two equations in the system (ODE) can be rewritten as:

$$\begin{cases} \dot{x_i} = \beta s_i \sum_{j \in N} [A_{ij}(1-l_i)(1-l_j)x_j] - (\gamma + \kappa)x_i \\ \dot{s_i} = -\beta s_i \sum_{j \in N} [A_{ij}(1-l_i)(1-l_j)x_j]. \end{cases}$$

We determine the value of $s_i(\infty)$ by integration of these equations over the entire epidemic period, which entails

$$\log\, s_i(\infty) - \log\, s_i(0) = -\beta \sum_{j\in N}[A_{ij}(1-l_i)(1-l_j)\int_0^\infty x_j d_t], \tag{A1}$$

$$s_i(\infty) - s_i(0) = \int_0^\infty (\dot{x_i} + \dot{s_i})dt = -(\gamma+\kappa)\int_0^\infty x_i d_t. \tag{A2}$$

We derive the outcome of the epidemic in terms of the ratio $\sigma_i = \frac{s_i(\infty)}{s_i(0)}$, which is approximately the probability of being susceptible and remaining uninfected at the end of the epidemic, $s_i(\infty)$, given that $s_i(0) \approx 1$. We use the column vector $\sigma = (\sigma_1, ..., \sigma_n)^T$ to express the size of the epidemic since the infected rate for agent i is $z_i = 1-\sigma_i$, and the final size of the epidemic in the whole population is $\sum_{j\in N} z_j N$. For each agent i, the attack rate z_i also equals $r_i(\infty) + d_i(\infty)$, since $x_i(t) \to 0$ when $t \to \infty$. Noting that $(1-\sigma_i)s_i(0) = s_i(0) - s_i(\infty)$, and substituting Eq.(A2) into Eq.(A1) yields the size of epidemic σ as a solution of the coupled implicit equations:

$$0 = \log\, \sigma_i + \sum_{j\in N}[\frac{\beta}{\gamma+\kappa}A_{ij}(1-l_i)(1-l_j)s_j(0)](1-\sigma_j) = \mathcal{H}_i(\sigma),\ i = 1, 2..., n. \tag{A3}$$

Recall that $\mathcal{M}_{ij}$, which is the (i,j)-entry in the next-generation matrix is $\frac{\beta}{\gamma+\kappa}A_{ij}(1-l_i)(1-l_j)$. With $s_i(0) \approx 1$ for all i, the final size equation (A3) can be written in matrix notation with the next-generation matrix $\mathcal{M}$, the coordinate-wise log-function, and the column null vector $\overline{0} = (0, ..., 0)^T$ as:

$$\overline{0} = \log\, \sigma + \mathcal{M}(\overline{1} - \sigma) = \mathcal{H}(\sigma), \tag{A4}$$

where $\overline{1} = (1, ..., 1)^T$. Now, taking the coordinate-wise exp of equation (A4) entails the alternative version of the final size equation in $z = \overline{1} - \sigma$:

$$z = \overline{1} - \exp(-\mathcal{M}z). \tag{A5}$$

Following Andreasen (2011), we interpret equation (A5) as a probabilistic identity as z_i is the probability that agent i becomes infected during the epidemic while $\exp(-\sum_{j\in N}\mathcal{M}_{ij}z_j)$ gives the probability of remaining susceptible during the entire epidemic. The question that remains is whether the final size equation (A4) admits a solution. It is unambiguous to show that the column vector $\sigma^0 = (1, ..., 1)^T$, which corresponds to the disease free equilibrium E_0, yields $\mathcal{H}(\sigma^0) = \overline{0}$, meaning that σ^0 is a solution to the problem (A4). However, more solutions might exist to the final size equation. Using the result

from Andreasen (2011, Theorem 2, p. 2313), we provide the adapted following proposition that specifies conditions for solutions to Eq.(A4).

Proposition 4 *Let $v_1, ..., v_n$ denote the set of eigenvectors and generalized eigenvectors of the next-generation matrix $\mathcal{M}$ and $u_1, ..., u_n$ the set of these vectors squared coordinate-wise. If each u_k is linearly independent of the set of all eigenvectors and generalized eigenvectors excluding v_k, then the final size equation (A4) has a single solution in the open unit $(0,1)^n$ if $R_0 > 1$ and none if $R_0 < 1$.*

Proof To prove Proposition 4, we use bifurcation theory in line with Andreasen (2011) by treating R_0 as a bifurcation parameter. We first show that if $R_0 < 1$, Eq.(A4) admits no solutions in the interior of $(0,1)^n$. Assume the contrary. Then there exists $\sigma \in (0,1)^n$ which solves Eq.(A4). By the Perron-Frobenius Theorem, we can choose the left eigenvector ω corresponding to the dominant eigenvalue of $\mathcal{M}$ (i.e., $\omega^T \mathcal{M} = R_0 \omega^T$) to have positive entries and satisfy $\omega^T \bar{1} = 1$. Taking the inner product of ω and Eq.(A4) yields:

$$\begin{aligned} 0 = \omega^T \bar{0} &= \omega^T \log \sigma + \omega^T \mathcal{M}(\bar{1} - \sigma) \\ &= \omega^T \log \sigma + R_0 \omega^T (\bar{1} - \sigma) \\ &\leq \log \omega^T \sigma + R_0(1 - \omega^T \sigma) \text{ by Jensen's inequality} \\ &\leq (R_0 - 1)(1 - \omega^T \sigma) < 0 \text{ by the inequality } \log y \leq y - 1, \end{aligned}$$

which is a contradiction. Therefore if $R_0 < 1$, Eq.(A4) admits no roots in the interior of $(0,1)^n$.

Assume that $R_0 > 1$. Let z^2 and $\log z$ denote the coordinate-wise operations on the vector. Let v_1 be a positive right eigenvector of $\mathcal{M}$ corresponding to R_0 (i.e., $\mathcal{M}v_1 = R_0 v_1$) and $u_1 = v_1^2$. Following Andreasen (2011), we perform an asymptotic expansion of Eq.(A4) in $(R_0 - 1)$ and we show the existence of a feasible root of Eq.(A4) in the form

$$1 - \sigma = z = (R_0 - 1)\xi_0 v_1 + (R_0 - 1)^2 \sum_k \xi_k v_k + O[(R_0 - 1)^3],$$

where the coefficients $\xi_0 \neq 0$ and ξ_2 to ξ_n are to be determined. Let ς_k be the subdominant eigenvalues of $\mathcal{M}$. We can rewrite and simplify Eq.(A4) to

$$\begin{aligned} 0 &= \mathcal{M}z + \log(1 - z) \\ &= \mathcal{M}z - z - \frac{1}{2}z^2 + \text{h.o.t.} \\ &= (R_0 - 1)^2 \xi_0 v_1 - \frac{1}{2}(R_0 - 1)^2 \xi_0^2 u_1 + (R_0 - 1)^2 \sum_k \xi_k(\varsigma_k - 1)v_k + O[(R_0 - 1)^3]. \end{aligned}$$

Keeping only terms of order $(R_0 - 1)^2$ and letting $\xi_k' = \frac{\xi_k}{\xi_0}$, it follows that ξ_0 and ξ_k' must solve the equation:

$$v_1 = \frac{1}{2}\xi_0 u_1 + \sum_k \xi_k'(1 - \varsigma_k)v_k.$$

Assuming that u_1 is linearly independent of the set of subdominant eigenvectors v_2 to v_n ensures the existence and uniqueness of the solution. Since v_1 is independent

of eigenvectors v_2 to v_n, it holds that $\xi_o \neq 0$, and from the reasoning above $\xi_0 > 0$. We have shown that there exists a small, positive solution in z, and consequently of a solution $\sigma = \overline{1} - z \in (0,1)^n$, for $0 < R_0 - 1 \ll 1$.

Note that except for the trivial solution $\sigma^0 = (1, ..., 1)^T$, Eq.(A4) has the same solutions as the vector-equation

$$0 = \mathcal{M}_{kk} + \sum_{j \neq k} \mathcal{M}_{kj} \frac{1-\sigma_j}{1-\sigma_k} + \frac{\log \sigma_k}{1-\sigma_k} = \sum_{j \neq k} \mathcal{M}_{kj} \frac{1-\sigma_j}{1-\sigma_k} + \frac{\log \sigma_k}{1-\sigma_k}, \; k = 1, ..., n, \quad \text{(A6)}$$

since $\mathcal{M}_{kk} = 0$, for $k = 1, .., n$. Considering the left-hand sides of Eq.(A6) as a vector-valued function $G(\sigma_1, ..., \sigma_n)$, and using a similar derivation as in Andreasen (2011, Lemma 3, pp. 2312–2313) , we can show that the determinant of the Jacobian of G is different than zero. The latter means that the number of solutions to $G = 0$ cannot change in the open unit-cube. Therefore, additional solutions to Eq.(A4) cannot arise through bifurcation in the interior of $(0,1)^n$.

Finally, we need to show that Eq.(A4) has no non-trivial solutions on the boundary of $(0,1)^n$. Assume the contrary. Then, there exists $\sigma \neq \sigma^0$ on the boundary of $(0,1)^n$ which solves Eq.(A4). It is direct that $\sigma_k \neq 0$ for all k. Similarly, there are some k for which $\sigma_k = 1$. Since $\log \sigma_k = 0$, from Eq.(A4), the expression on the kth row gives $\sum_l \mathcal{M}_{kl}(1 - \sigma_l) = 0$ implying that $\sigma_l = 1$ for all l. The latter contradicts the fact that $\sigma \neq \sigma^0$.

To conclude the proof, note that we exclude the possibility of additional solutions crossing through the trivial root $\sigma^0 = (1, ..., 1)^T$. In fact, following Andreasen (2011), additional bifurcation at σ^0 may occur only as subdominant eigenvalues pass through unity. However, from the Perron-Frobenious theorem, the associated eigenvectors to the eigenvalues can not be positives on all entries. Using the same reasoning as above to the subdominant eigenvector, we can prove that such solutions cannot enter $(0,1)^n$. Therefore, we conclude the proof. □

Appendix B Theoretical derivations for the planning problem

The current Hamiltonian of problem (2) is given as:

$$\begin{aligned}\mathcal{H}_c(l, x, r, d, s, \mu^1, \mu^2, \mu^3, \mu^4) = &\sum_{i \in N} W_i(k_i, s_i, x_i, r_i, d_i, l_i) + \sum_{i \in N} \mu_i^1 f_i + \gamma \sum_{i \in N} \mu_i^2 x_i \\ &+ \kappa \sum_{i \in N} \mu_i^3 x_i + \sum_{i \in N} \mu_i^4 [-f_i - (\gamma + \kappa) x_i],\end{aligned}$$

where μ_i^j $(j = 1, .., 4)$, for each $i \in N$, are the costate variables. Given the inequality constraints $\dot{x_i} \leq \lambda$, and the constraints $l_i(t) \in [0,1]$, we augment the current Hamiltonian $\mathcal{H}_c$ into the current Lagrangian function:

$$\begin{aligned}\mathcal{L}_c(l, x, r, d, s, \mu^1, \mu^2, \mu^3, \mu^4, \theta^1, \theta^2, \theta^3) = &\sum_{i \in N} W_i(k_i, s_i, x_i, r_i, d_i, l_i) + \sum_{i \in N} \mu_i^1 f_i \\ &+ \gamma \sum_{i \in N} \mu_i^2 x_i + \kappa \sum_{i \in N} \mu_i^3 x_i + \sum_{i \in N} \mu_i^4 [-f_i - (\gamma + \kappa) x_i] \\ &+ \sum_{i \in N} \theta_i^1 (\lambda - f_i) + \sum_{i \in N} \theta_i^2 l_i + \sum_{i \in N} \theta_i^3 (1 - l_i),\end{aligned}$$

where the parameters θ^j, $j = 1, 2, 3$, are Lagrange multipliers. We can also rewrite $\mathcal{L}_c$ as:

$$\begin{aligned}\mathcal{L}_c(l, x, r, d, s, \mu^1, \mu^2, \mu^3, \mu^4, \theta^1, \theta^2, \theta^3) = & \sum_{i\in N} W_i(k_i, s_i, x_i, r_i, d_i, l_i) + \sum_{i\in N}(\mu_i^1 - \mu_i^4 - \theta_i^1) f_i \\ & + \gamma \sum_{i\in N} \mu_i^2 x_i + \kappa \sum_{i\in N} \mu_i^3 x_i - (\gamma+\kappa) \sum_{i\in N} \mu_i^4 x_i \\ & + \lambda \sum_{i\in N} \theta_i^1 + \sum_{i\in N} \theta_i^2 l_i + \sum_{i\in N} \theta_i^3 (1 - l_i).\end{aligned}$$

The first-order conditions for maximizing $\mathcal{L}_c$ call for, assuming interior solutions,

$$\frac{\partial \mathcal{L}_c}{\partial l_k} = 0, \; k \in N, \tag{B7}$$

as well as for each $k \in N$:

$$\frac{\partial \mathcal{L}_c}{\partial \theta_k^1} = \lambda - \dot{x_k} \geq 0, \qquad \theta_k^1 \geq 0, \qquad \theta_k^1 \frac{\partial \mathcal{L}_c}{\partial \theta_k^1} = \theta_k^1(\lambda - \dot{x_k}) = 0, \tag{B8}$$

$$\frac{\partial \mathcal{L}_c}{\partial \theta_k^2} = l_k \geq 0, \qquad \theta_k^2 \geq 0, \qquad \theta_k^2 \frac{\partial \mathcal{L}_c}{\partial \theta_k^2} = \theta_k^2 l_k = 0, \text{ and} \tag{B9}$$

$$\frac{\partial \mathcal{L}_c}{\partial \theta_k^3} = 1 - l_k \geq 0, \qquad \theta_k^3 \geq 0, \qquad \theta_k^3 \frac{\partial \mathcal{L}_c}{\partial \theta_k^3} = \theta_k^3(1 - l_k) = 0. \tag{B10}$$

Finally, the other maximum-principle conditions that include the dynamics for state and co-state variables are, for $k \in N$:

$$\dot{x_k} = \frac{\partial \mathcal{L}_c}{\partial \mu_k^1} \qquad \dot{r_k} = \frac{\partial \mathcal{L}_c}{\partial \mu_k^2} \qquad \dot{d_k} = \frac{\partial \mathcal{L}}{\partial \mu_k^3} \qquad \dot{s_k} = \frac{\partial \mathcal{L}_c}{\partial \mu_k^4}, \text{ and}$$

$$\dot{\mu_k^1} = \delta \mu_k^1 - \frac{\partial \mathcal{L}_c}{\partial x_k} \quad \dot{\mu_k^2} = \delta \mu_k^2 - \frac{\partial \mathcal{L}_c}{\partial r_k} \quad \dot{\mu_k^3} = \delta \mu_k^3 - \frac{\partial \mathcal{L}_c}{\partial d_k} \quad \dot{\mu_k^4} = \delta \mu_k^4 - \frac{\partial \mathcal{L}_c}{\partial s_k} \tag{B11}$$

Recall that $f_i(x_i, r_i, d_i, l_i) = \beta(1-x_i-r_i-d_i)(1-l_i) \sum_{j\neq i} [A_{ij}(1-l_j)x_j] - (\gamma+\kappa)x_i$. Then,

$$\frac{\partial f_i}{\partial l_k} = \begin{cases} -\beta(1 - x_i - r_i - d_i) \sum_{j\neq i} [A_{ij}(1 - l_j)x_j] & \text{if } k = i \\ -\beta(1 - x_i - r_i - d_i)(1 - l_i)A_{ik}x_k & \text{if } k \neq i \end{cases}$$

$$\frac{\partial f_i}{\partial x_k} = \begin{cases} -\beta(1 - l_i) \sum_{j\neq i} [A_{ij}(1 - l_j)x_j] - (\gamma + \kappa) & \text{if } k = i \\ \beta(1 - x_i - r_i - d_i)(1 - l_i)(1 - l_k)A_{ik} & \text{if } k \neq i \end{cases}$$

$$\frac{\partial f_i}{\partial r_k} = \frac{\partial f_i}{\partial d_k} = \begin{cases} -\beta(1 - l_i) \sum_{j\neq i} [A_{ij}(1 - l_j)x_j] & \text{if } k = i \\ 0 & \text{if } k \neq i \end{cases}$$

We also recall that $W_i(k_i, s_i, x_i, r_i, d_i, l_i) = p_i y_i(k_i, s_i, x_i, r_i, d_i, l_i) - w_i h_i(s_i, x_i, r_i, d_i, l_i)$. Therefore, for each i and k, and for each $u \in \{s_k, x_k, r_k, d_k, l_k\}$, it holds that

$$\frac{\partial W_i}{\partial u} = \begin{cases} p_i \frac{\partial y_i}{\partial u} - w_i \frac{\partial h_i}{\partial u} & \text{if } k = i \\ 0 & \text{if } k \neq i \end{cases} \tag{B12}$$

Therefore, for each $k \in N$, we can write $\frac{\partial \mathcal{L}_c}{\partial l_k}$ as:

$$\begin{aligned}\frac{\partial \mathcal{L}_c}{\partial l_k} &= \sum_{i\in N} \frac{\partial W_i}{\partial l_k} + \sum_{i\in N} (\mu_i^1 - \mu_i^4 - \theta_i^1)\frac{\partial f_i}{\partial l_k} + \theta_k^2 - \theta_k^3 \\ &= \frac{\partial W_k}{\partial l_k} + \sum_{i\in N} (\mu_i^1 - \mu_i^4 - \theta_i^1)\frac{\partial f_i}{\partial l_k} + \theta_k^2 - \theta_k^3 \text{ using } (B12) \\ &= p_k \frac{\partial y_k}{\partial l_k} - w_k \frac{\partial h_k}{\partial l_k} + \sum_{i\in N} (\mu_i^1 - \mu_i^4 - \theta_i^1)\frac{\partial f_i}{\partial l_k} + \theta_k^2 - \theta_k^3\end{aligned} \tag{B13}$$

Hence, using the first-order conditions (B7), equation (B13) becomes:

$$0 = p_k \frac{\partial y_k}{\partial l_k} - w_k \frac{\partial h_k}{\partial l_k} + \sum_{i\in N} (\mu_i^1 - \mu_i^4 - \theta_i^1)\frac{\partial f_i}{\partial l_k} + \theta_k^2 - \theta_k^3.$$

Using the other conditions from (B11) and using (B12):

$$\dot{\mu_k^1} = \delta\mu_k^1 - \frac{\partial \mathcal{L}_c}{\partial x_k} = \delta\mu_k^1 - p\frac{\partial y_k}{\partial x_k} + w_k \frac{\partial h_k}{\partial x_k} - \gamma\mu_k^2 - \kappa\mu_k^3 + (\gamma+\kappa)\mu_k^4 - \sum_{i\in N} (\mu_i^1 - \mu_i^4 - \theta_i^1)\frac{\partial f_i}{\partial x_k}. \tag{B14}$$

Similarly, using (B11), we get:

$$\dot{\mu_k^2} = \delta\mu_k^2 - \frac{\partial \mathcal{L}_c}{\partial r_k} = \delta\mu_k^2 - p\frac{\partial y_k}{\partial r_k} + w_k \frac{\partial h_k}{\partial r_k} - \sum_{i\in N} (\mu_i^1 - \mu_i^4 - \theta_i^1)\frac{\partial f_i}{\partial r_k} \text{ using } (B12), \tag{B15}$$

$$\dot{\mu_k^3} = \delta\mu_k^3 - \frac{\partial \mathcal{L}_c}{\partial d_k} = \delta\mu_k^3 - p\frac{\partial y_k}{\partial d_k} + w_k \frac{\partial h_k}{\partial d_k} - \sum_{i\in N} (\mu_i^1 - \mu_i^4 - \theta_i^1)\frac{\partial f_i}{\partial d_k} \text{ using } (B12), \tag{B16}$$

and

$$\dot{\mu_k^4} = \delta\mu_k^4 - \frac{\partial \mathcal{L}_c}{\partial s_k} = \delta\mu_k^4 - p\frac{\partial y_k}{\partial s_k} + w_k \frac{\partial h_k}{\partial s_k}. \tag{B17}$$

Appendix C Proofs of Theoretical Results

C.1 Proof of Proposition 1

Given that $s_i = 1 - x_i - r_i - d_i$, for each $i \in N$, we can rewrite (ODE) as:

$$(\text{ODE}): \begin{cases} \dot{x_i} = \beta(1 - x_i - r_i - d_i)(1 - l_i)\sum_{j\in N}[A_{ij}(1 - l_j)x_j] - (\gamma + \kappa)x_i \\ \dot{s_i} = -\beta(1 - x_i - r_i - d_i)(1 - l_i)\sum_{j\in N}[A_{ij}(1 - l_j)x_j] \\ \dot{r_i} = \gamma x_i \\ \dot{d_i} = \kappa x_i \end{cases}$$

Consider the vector-valued function $f_i(t, X_i) = (f_{i1}(t, X_i), f_{i2}(t, X_i), f_{i3}(t, X_i), f_{i4}(t, X_i))^T$, where

$$\begin{aligned} f_{i1}(t, X_i) &= \beta(1 - x_i - r_i - d_i)(1 - l_i)\sum_{j\in N}[A_{ij}(1 - l_j)x_j] - (\gamma + \kappa)x_i \\ f_{i2}(t, X_i) &= -\beta(1 - x_i - r_i - d_i)(1 - l_i)\sum_{j\in N}[A_{ij}(1 - l_j)x_j] \end{aligned}$$

$$f_{i3}(t, X_i) = \gamma x_i \text{ and}$$
$$f_{i4}(t, X_i) = \kappa x_i.$$

The function f_i is a continuously differentiable function, for each $i \in N$. Consequently, the ODE admits a unique solution, $\mathcal{S}^*(l, A, \beta, \gamma, \kappa, X_0)$, thanks to the theorem of existence and uniqueness of a solution for first-order general ordinary differential equations, where $l = (l_i)_{i \in N} \in [0, 1]^n$ is a vector of individual lockdown probabilities.

C.2 Proof of Proposition 2

Let $\mathcal{J} = \mathcal{A} - \mathcal{B}$. We denote, $s(\mathcal{J})$, the maximum real part of all the eigenvalues of the matrix $\mathcal{J}$ (the spectral abscissa of $\mathcal{J}$). Following Van den Driessche and Watmough (2002, Lemma 1, p. 32), the DFE E_0 of system (ODE) is locally-asymptotically stable if all the eigenvalues of the matrix $\mathcal{J}$ have negative real parts (i.e., $s(\mathcal{J}) < 0$), and unstable if any eigenvalue of $\mathcal{J}$ has a positive real part (i.e., $s(\mathcal{J}) > 0$). A matrix $A = [A_{ij}]$ has the Z-sign pattern if $A_{ij} \leq 0$ for all $i \neq j$. It is direct that the matrix $\mathcal{B}$ has the Z-sign pattern. The eigenvalues of $\mathcal{B}$ have positive real parts. Thus, $\mathcal{B}$ is a non-singular M-matrix (for additional information on M-matrices, we refer to Van den Driessche and Watmough (2002) and the references therein). Also, the matrix $-\mathcal{J}$ have the Z-sign pattern. Thus, $s(\mathcal{J}) < 0$ if and only if $-\mathcal{J}$ is a non-singular M-matrix. Since $\mathcal{M}$ is non-negative, then $-\mathcal{J}\mathcal{B}^{-1} = I - \mathcal{M}$ also has the Z-sign pattern. Applying Van den Driessche and Watmough (2002, Lemma 5, p. 47), $-\mathcal{J}$ is a non-singular M-matrix if and only if $I - \mathcal{M}$ is a non-singular M-matrix. Since the matrix $\mathcal{M}$ is non-negative, all the eigenvalues of $\mathcal{M}$ have magnitude less than or equal to $\rho(\mathcal{M})$. Thus, $I - \mathcal{M}$ is a non-singular M-matrix if and only if $\rho(\mathcal{M}) < 1$. Hence, $s(\mathcal{J}) < 0$ if and only if $R_0 = \rho(\mathcal{M}) < 1$. Similarly, it follows that $s(\mathcal{J}) = 0$ if and only if $-\mathcal{J}$ is a singular M-matrix. The latter is equivalent to $I - \mathcal{M}$ is a singular M-matrix (applying Van den Driessche and Watmough (2002, Lemma 6, p. 47)). Thus, $I - \mathcal{M}$ is a singular M-matrix if and only $\rho(\mathcal{M}) = 1$. Consequently, $s(\mathcal{J}) = 0$ if and only if $\rho(\mathcal{M}) = 1$. Therefore, it follows that $s(\mathcal{J}) > 0$ if and only if $R_0 = \rho(\mathcal{M}) > 1$.

C.3 Proof of Proposition 3

We denote $f_i(k_i, s_i, x_i, r_i, d_i, l_i) \equiv f_i(k_i, x_i, r_i, d_i, l_i) = \beta[1 - x_i - r_i - d_i](1 - l_i) \sum_{j \in N} [A_{ij}(1 - l_j)x_j] - (\gamma + \kappa)x_i$, and $W_i(k_i, s_i, x_i, r_i, d_i, l_i) = p_i y_i(k_i, s_i, x_i, r_i, d_i, l_i) - w_i h_i(s_i, x_i, r_i, d_i, l_i)$. The function $l_i : t \longrightarrow l_i(t) \in [0, 1]$ is continuous. The function W_i, and the objective function in (2) are continuous and differentiable. Moreover, f_i and the right-hand sides of the laws of motion in (2) are all continuous and differentiable. It follows that the problem (2) admits a unique optimal path $\{l^*(t)\}$ of the control variable (and the states $\{x^*(t), r^*(t), d^*(t), s^*(t)\}$, given the initial conditions X_0 and the laws of motion).

Appendix D Optimal Dynamics with Simulations

We obtain our optimal lockdown dynamics by solving the planning problem described in Eq.(2). The simulation process involves solving Eqs.(B7) to (B11), and (B14) to

(B17). The lockdown dynamics yield the disease and economic costs dynamics. We use the software **Matlab_2020a** and the function **ode45** to solve the system of ordinary differential equations describing the N-SIRD epidemiological model. The existence and uniqueness of the solution for our epidemiological model and planning problem are established in Propositions 1 and 3, respectively. These conditions ensure that the output from our simulations is the appropriate approximation of the N-SIRD optimal dynamics. As initial inputs in the simulations, we specify the adjacency matrix A, representing the social network structure, and randomly impose 10% of infected agents. At the initial period, there is no agent in lockdown. For each period $t \in \{1, 2, ..., 80\}$, the simulation program optimally produces individual probabilities for each of our variables of interest. Then, we represent the average probability in the sample for each point in time t in Figs. 1, 3, and 4. We can view these dynamics as representative of the population dynamics and thus useful for policy analysis and decision making.

Appendix E Definitions of Network Metrics

We recall that the network A is a symmetric $n \times n$ weighted adjacent matrix (A_{ij}). An agent's *degree centrality* χ_i equals the total number of other agents directly connected to agent i (i.e., the number of agent i's neighbors): $\chi_i = \sum_{j=1}^{n} A_{ij}$. *Eigenvector centrality* ν_i measures the extent to which agent i is connected to other highly connected agents in the network A: $\nu_i = \frac{1}{e} \sum_{j=1}^{n} A_{ij}\nu_j$. The eigenvector centrality is computed using the principal eigenvector ν of the adjacent matrix A, that we can write in matrix notation as $A\nu = e\nu$, where ν is a column vector with n entries. The eigenvector centrality reflects the notion that connections to highly connected agents are more important. Agent i's betweenness centrality, b_i, measures the fraction of shortest paths passing through agent i: $b_i = \sum_{j,k} \frac{\sigma^i_{jk}}{\sigma_{jk}}$, where σ_{jk} is the total number of shortest paths from agents j to k, and σ^i_{jk} is the number of those paths that pass through agent i. Agent i's *closeness centrality*, c_i, measures how close is the agent to all other agents in the network A: $c_i = \frac{1}{\sum_j d(i,j)}$, where $d(i, j)$ is the distance (or shortest path) between agents i and j. It follows from these definitions that the degree centrality is less based on network configuration than the other centrality measures.

Appendix F Estimating λ: Additional Details

F.1 Calibrate a U.S. nursing home production function

In our study, we use data from several sources. Our primary source of external data comes from the Protect Nursing Homes project and the replication package made publicly available by M.K. Chen et al. (2021). Table 2 describes the relevant parameters, their sources, and their use in our simulations and empirical analyses. For calibration, we assume that the production structure is homogeneous within a U.S. state. To estimate the production function for a nursing home i in a U.S. state, we assume a Cobb-Douglas function $y_i = k_i^{\alpha^1} h_i^{\alpha^2}$, where y_i is the total number of residents who receive care (output), k_i is the total number of beds (proxy for

capital), and h_i is the number of occupied beds (a proxy for the labor demand). We assume that a nursing home hires staff according to the demand for its services, and the latter is closely related to the number of occupied beds. We estimate the elasticity α^1 and α^2 by assuming a log-log specification and controlling for a series of factors, including overall rating, County SSA, CMS quality rating, urban/rural, and for-profit/not-for-profit. We use the following simple log-log econometric equation:

$$log(y_i) = \alpha^0 + \alpha^1 log(k_i) + \alpha^2 log(h_i) + \beta X_i + e_i,$$

where X_i represents exogenous nursing home i's characteristics and e_i is the error term. The estimates of the parameter α^1 ($\alpha^1 = \alpha$, $\alpha^2 \approx 1-\alpha$) for each U.S. state and other state's parameters that we use to simulate the N-SIRD model are presented in Table F1.

Table F1: Data used to simulate the N-SIRD model for each U.S. state

U.S. States	Wage/hour	Price/hour	Case/100000	Death/100000	R_0	α^1	Min. Degree
AL	33	9.29	365.9	59.3	0.93	0.3853637	13
AR	43	11.04	281.4	59.6	0.95	0.5218234	13
AZ	35	8.79	241.2	45.8	0.97	0.5852448	13
CA	52	15.37	274.8	51.8	0.86	0.6297461	13
CO	42	13.08	109.6	38.4	0.92	0.538735	13
CT	46	18.81	345	100	0.96	0.6257474	13
DC	42	17.07	229.9	56.3	0.92	1.002931	1
DE	52	19.30	188.3	55.3	0.97	0.7739902	1
FL	39	13.19	283	53.1	0.97	0.6614283	22
GA	38	9.64	356.1	73.7	0.84	0.4615252	22
IA	38	12.26	131.2	31	0.92	0.2876858	1
ID	40	9.44	162	22.8	0.87	0.2217902	1
IL	39	11.41	209	52.8	0.87	0.4060938	11
IN	36	9.61	159.8	59	0.88	0.2871411	11
KS	35	9.44	83.6	16	0.96	0.3383333	11
KY	34	10.67	162.4	34.9	1.01	0.331612	11
LA	34	7.85	418.6	85.5	0.89	0.2518069	11
MA	42	14.27	356.1	125.1	0.94	0.76337	11
MD	45	14.31	263.1	62.4	0.94	0.6189594	11
ME	47	18.19	48.3	9	0.96	0.7124791	1
MI	39	13.08	138.2	48.8	0.9	0.6715142	9
MN	44	16.16	100.9	33.8	0.94	0.5657483	9
MO	32	9.61	180.6	30.8	0.94	0.2763414	9
MS	36	7.73	367	74.9	1.08	0.6377482	1
MT	41	11.12	23.5	4.7	0.87	0.0505241	1
NC	38	10.66	221.9	46.1	0.92	0.5917483	NaN
ND	45	14.23	102.3	15	1.09	0.4858396	2
NE	45	15.21	94.2	26.4	0.94	0.3416526	2
NH	47	15.94	141.9	38.3	0.95	0.5850638	2
NJ	42	11.16	365.8	120.1	1.03	0.7126257	2
NM	46	17.38	138.6	50.1	0.84	0.549336	2
NV	38	10.83	209.9	26.4	0.95	0.7162963	2
NY	38	17.16	145.2	50.5	0.91	0.7638234	2
OH	38	11.04	149.2	34.9	0.88	0.5926255	2
OK	36	7.77	148.2	22.2	1.05	0.4150358	2
OR	48	15.02	74.5	13.6	0.94	0.2144981	2
PA	39	14.55	207.1	66.2	0.88	0.6404236	9
RI	46	13.74	288.8	86.6	0.92	0.9319015	9
SC	37	10.57	342.2	63.1	0.9	0.5003951	9
SD	35	10.11	78.9	14.4	0.94	0.3584688	1
TN	34	10.24	166.5	24.8	0.87	0.2476998	9
TX	38	8.59	325.7	62	0.97	0.3152237	22
UT	37	11.24	134	31.9	0.98	0.3648363	NaN
VA	41	13.86	192.3	46.2	1.05	0.6377195	NaN
VT	41	11.86	35	11.1	1.11	0.6885093	2
WA	47	14.72	152.7	38	0.97	0.6368927	9
WI	35	16.31	64	12.4	0.91	0.2780716	9
WV	41	12.67	101.7	17.8	0.87	0.2662697	9
WY	42	11.71	8.4	2.2	0.99	0.2333506	1

Note: Min. Degree is the minimum degree centrality of the nursing homes kept in the sample to ensure the the next-generation matrix, $\mathcal{M}$ can be computed. "NaN" in the table means "Non Available." For these three U.S. states, there was no degree centrality level for which we can simulate the N-SIRD model with the available epidemiological and economic parameters.

F.2 Estimation of the Tolerable Infection Incidence Parameters

Our study uses the simulated minimum distance estimator to estimate the tolerable COVID-19 infection incidence value for all U.S. states in our sample. Given the lack of data on daily COVID-19 deaths in the nursing home data provided by M.K. Chen et al. (2021), we use the New York Times' daily COVID-19 death count for each U.S. state between May 31 and August 16, 2020. Following National Center for Health Statistics (2020), Freed, Cubanski, Neuman, Kates, and Michaud (2020), and Powell, Bellin, and Ehrlich (2020), we assume that 80% of U.S. COVID-19 deaths on average are seniors (65 years and older). We use these figures as our observed outcome.

Let us index a U.S. state in M.K. Chen et al. (2021)'s data set by $s \in \overline{S}$, with $\overline{S} = \{1, ..., 49\}$. Let d_{ts} denote the number of COVID-19 deaths observed at time $t = 1, ..., \bar{t}$ in the U.S. state $s \in \overline{S}$. For each value of the tolerable infection incidence λ, we can simulate death dynamics denoted as $\hat{d}_{ts}(\lambda)$. Since our simulations are deterministic, there is no random shock in our model. Thus, repeating the simulations with the same initial conditions produce the same results. For each U.S. state, we estimate the parameter that we denote as $\hat{\lambda}_s$ by solving the following minimization problem:

$$\hat{\lambda}_s = argmin \left\{ \sum_{t=1}^{\bar{t}} (\hat{d}_{ts}(\lambda) - d_{ts})^2 \right\}, \ \lambda \in [0, 1]. \tag{F18}$$

Existing literature on simulated minimum distance estimators (e.g., Gertler and Waldman (1992), and Forneron and Ng (2018)) suggests that $\hat{\lambda}_s$ is a consistent estimator of the tolerable COVID-19 infection incidence level for each U.S. state. The simulated minimum distance produces $\hat{\lambda}_s$ for 26 U.S. states. For the remaining 23 U.S. states, the parameter λ is not identified. This group of states can be divided into two. The first group consists of three states, NC, UT, and VA. For these U.S. states, the available epidemiological parameters and the data of their nursing home networks do not support our model. This usually occurs when the next-generation matrix, $\mathcal{M}$, cannot be obtained. We can refer to Proposition 2, which studies the asymptotic stability of the system (ODE) at the disease-free equilibrium E_0, and provides conditions for which an infection in a fully susceptible population could generate an epidemic outbreak. The proof of Proposition 2 in Appendix C.2 transforms such conditions into properties (e.g., non-singularity) placed on the next-generation matrix, $\mathcal{M}$, which also depends on the network structure of nursing homes in the U.S. state. For the second group which consists of the remaining 20 U.S. states, it is impossible for us to exclude zero tolerable infection tolerance (i.e., $\lambda = 0$) or any other level $\lambda \in]0, 1]$. Indeed, the estimation procedure always returns the initial value proposed, suggesting a flat objective function. We conjecture that the main reason that may justify this outcome is data quality. Indeed, the raw daily COVID-19 death count data from the New York Times is not specifically collected for the residents of nursing homes or for the population of seniors in the state. Because of data availability issues, and following National Center for Health Statistics (2020), Freed et al. (2020), and Powell et al. (2020), we assume that approximately 80% of daily U.S. COVID-19 deaths come from nursing homes. The death dynamics will match in U.S. states where most seniors are in nursing homes and their daily death counts follow the same trend as the state's COVID-19 death count. This means that in practice, there will be a potential mismatch between the simulation-based dynamic and the raw data dynamic.

Appendix G Robustness Checks

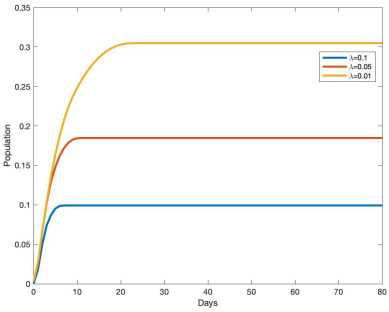

(a) Dynamics of lockdown

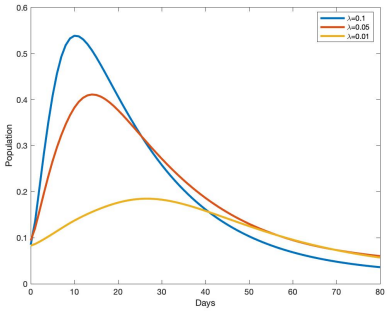

(b) Dynamics of infection

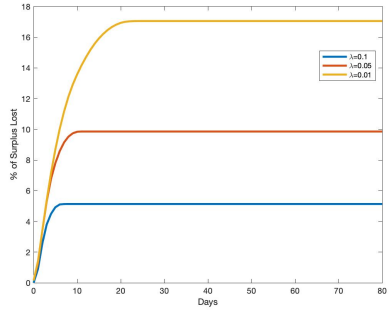

(c) Dynamics of economic Cost

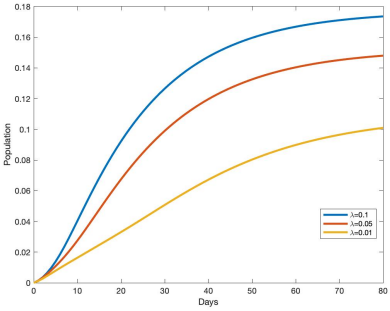

(d) Dynamics of death

Fig. G1: Health versus wealth tradeoff in a scale-free network. Note: We perform three sets of simulations with three different values of the tolerable infection incidence λ: 0.01, 0.05, and 0.1. The results are displayed in a two-dimensional graphic, with days on the horizontal axis, and the percentage of population affected for the variable (infection, lockdown, or death) illustrated on the vertical axis. In each period, a point in the graphic represents the average value of individual probabilities. For the economic cost, the vertical axis represents the percentage of economic surplus lost relative to the economy without the pandemic. Each graph shows three curves corresponding to three dynamics for a single variable of interest for a given value of λ. All variability within each curve in each graph is a result of the stochastic nature of transmission and not variation in the network or λ.

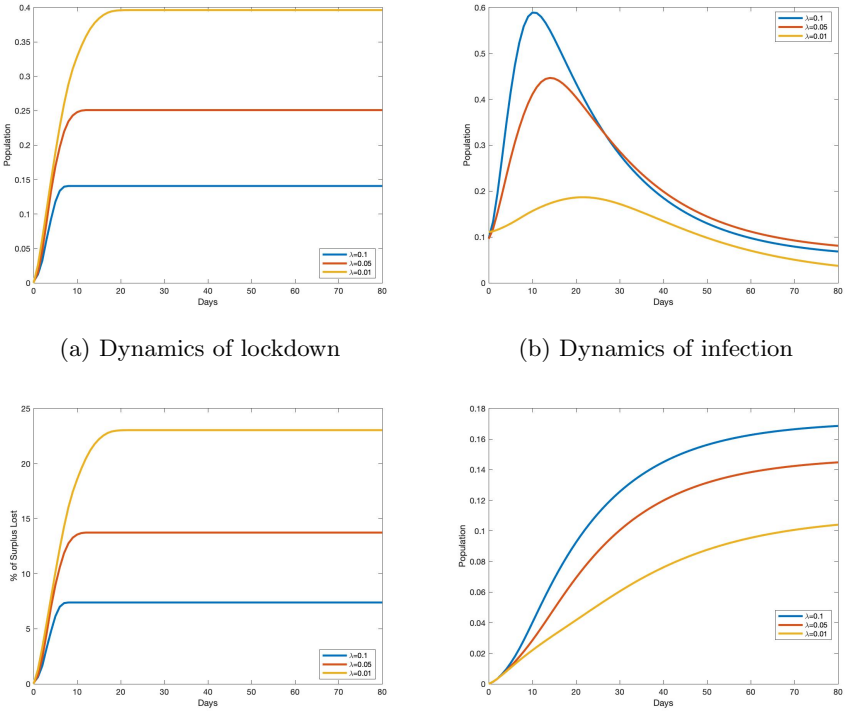

(a) Dynamics of lockdown

(b) Dynamics of infection

(c) Dynamics of economic Cost

(d) Dynamics of death

Fig. G2: Health versus wealth tradeoff in a random network. Note: We perform three sets of simulations with three different values of the tolerable infection incidence λ: 0.01, 0.05, and 0.1. The results are displayed in a two-dimensional graphic, with days in the horizontal axis, and the percentage of population affected for the variable (infection, lockdown, or death) illustrated on the vertical axis. In each period, a point in the graphic represents the average value of individual probabilities. For the economic cost, the vertical axis represents the percentage of economic surplus lost relative to the economy without the pandemic. Each graph shows three curves corresponding to three dynamics for a single variable of interest for a given value of λ. All variability within each curve in each graph is a result of the stochastic nature of transmission and not variation in the network or λ.

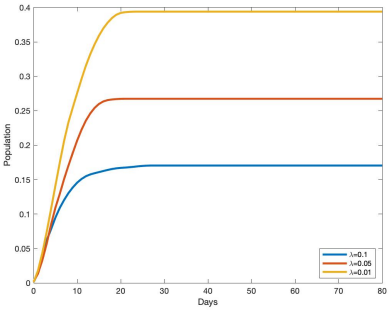

(a) Dynamics of lockdown

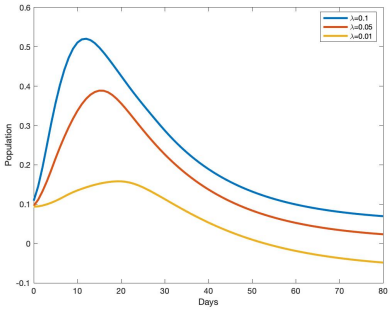

(b) Dynamics of Infection

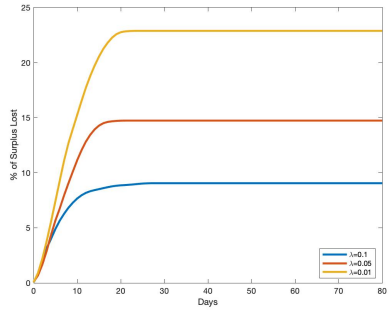

(c) Dynamics of Economic Cost

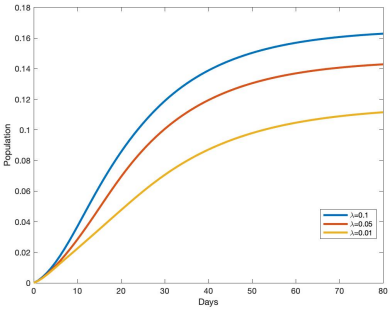

(d) Dynamics of Death

Fig. G3: Health versus wealth tradeoff in a lattice network. Note: We perform three sets of simulations with three different values of the tolerable infection incidence λ: 0.01, 0.05, and 0.1. The results are displayed in a two-dimensional graphic, with days in the horizontal axis, and the percentage of population affected for the variable (infection, lockdown, or death) illustrated on the vertical axis. In each period, a point in the graphic represents the average value of individual probabilities. For the economic cost, the vertical axis represents the percentage of economic surplus lost relative to the economy without the pandemic. Each graph shows three curves corresponding to three dynamics for a single variable of interest for a given value of λ. All variability within each curve in each graph is a result of the stochastic nature of transmission and not variation in the network or λ.

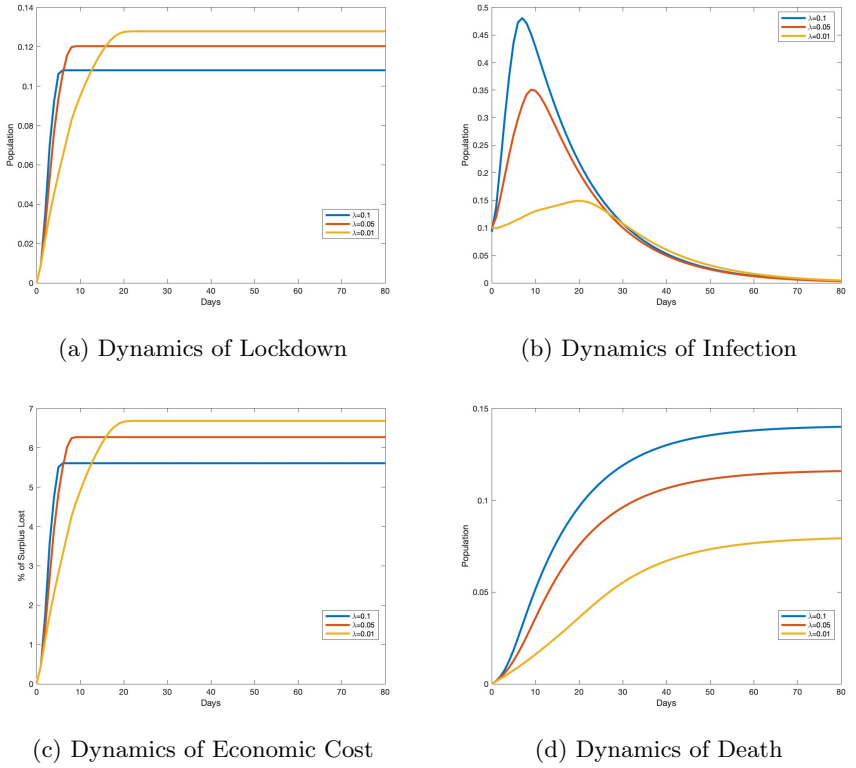

(a) Dynamics of Lockdown

(b) Dynamics of Infection

(c) Dynamics of Economic Cost

(d) Dynamics of Death

Fig. G4: Health versus wealth tradeoff with COVID-19 Delta variant parameters in a small-world network. Note: We perform three sets of simulations with three different values of the tolerable infection incidence λ: 0.01, 0.05, and 0.1. The epidemiological parameters are set to match the transmissibility of the COVID-19 Delta variant ($R_0 = 5.08$; see Liu and Rocklöv (2021)). The infectious period is set to 14 days and the recovery and death rates are left unchanged. The results are displayed in a two-dimensional graphic, with days on the horizontal axis, and the percentage of population affected for the variable (infection, lockdown, or death) on the vertical axis. In each period, a point in the graphic represents the average value of individual probabilities. For the economic cost, the vertical axis represents the percentage of economic surplus lost relative to the economy without the pandemic. Each graph shows three curves corresponding to three dynamics for a single variable of interest for a given value of λ. All variability within each curve in each graph is a result of the stochastic nature of transmission and not variation in the network or λ.

Table G2: Network centrality and lockdown probability in lattice, random, and scale-free network configurations

		$\lambda = 0.1$			$\lambda = 0.05$			$\lambda = 0.01$		
		Lattice	Random	Scale Free	Lattice	Random	Scale Free	Lattice	Random	Scale Free
Eigenvalue	corr	-2.09E-16	0.1988	0.2733	-1.39E-15	0.2049	0.0203	-1.15E-15	0.2045	0.015
	p-value	1	2.26E-10	1.35E-18	1	6.17E-11	0.5223	1	6.70E-11	0.6362
Degree	corr	NaN	0.2339	0.4105	NaN	0.2389	0.1239	NaN	0.2731	0.1302
	p-value	NaN	6.81E-14	6.23E-42	NaN	1.91E-14	8.55E-05	NaN	1.47E-18	3.62E-05
Betweenness	corr	0.0034	0.2167	0.2647	6.31E-04	0.2116	0.0437	0.0015	0.2348	0.0434
	p-value	0.915	4.32E-12	1.72E-17	0.9841	1.37E-11	0.1675	0.9617	5.39E-14	0.1701
Closeness	corr	2.03E-16	0.2202	0.4006	1.39E-15	0.2426	0.0954	1.15E-15	0.2509	0.0591
	p-value	1	1.91E-12	7.83E-40	1	7.35E-15	0.0025	1	7.99E-16	0.0618

Note: The p-value for each centrality measure is for the test of the hypothesis H_0 $\rho = 0$ vs H_1 $\rho \neq 0$. Not all correlations are statistically significant. The label "NaN" means "Non available." In the lattice network, all individuals have the same degree. Thus, we can't compute the correlation between the degree centrality and optimal lockdown probabilities. For the random network, we observe a strong correlation between centrality measures and the optimal lockdown probabilities. However, there is no relationship between the tolerable infection incidence and the centrality lockdown nexus. The lockdown dynamics and correlations in the scale-free and small-world networks move in the same direction.

Table G3: Network centrality and lockdown probability in a small-world network with COVID-19 Delta variant parameters

λ	Eigenvalue		Degree		Betweenes		Closeness	
	corr	p-value	corr	p-value	corr	p-value	corr	p-value
0.1	**0.2121**	1.24E-11	**0.2769**	4.67E-19	**0.231**	1.39E-13	**0.2277**	3.17E-13
0.05	**0.2055**	5.38E-11	**0.2696**	4.04E-18	**0.2296**	2.00E-13	**0.2386**	2.09E-14
0.01	**0.1012**	0.0014	**0.1829**	5.66E-09	**0.1334**	2.30E-05	**0.1513**	1.53E-06

Note: Table G3 illustrates the correlation (corr) between measures of centrality and average optimal lockdown probability in a small-world network with COVID-19 Delta variant parameters for three values of λ. The p-value for each centrality measure is for the test of the hypothesis H_0 $\rho = 0$ vs H_1 $\rho \neq 0$.

Table G4: Estimation of laissez-faire policies in U.S. nursing homes with degree centrality

	(1)	(2)	(3)	(4)	(5)
λ	0.197	1.129**	1.700**	-0.451	1.601**
	(0.57)	(3.02)	(2.58)	(-0.89)	(2.19)
Degree Centrality	0.0616***	0.0900***	0.0622***	0.0612***	0.0903***
	(6.34)	(6.79)	(6.41)	(6.29)	(6.75)
County_ssa	-0.000773	-0.000824	-0.000501	-0.000786	-0.000598
	(-1.09)	(-1.17)	(-0.70)	(-1.11)	(-0.84)
D_Profit	0.208*	0.211*	0.210*	0.0772	0.0358
	(1.76)	(1.79)	(1.78)	(0.56)	(0.26)
$\lambda\times$ Degree Centrality		-0.169***			-0.170***
		(-3.12)			(-3.07)
$\lambda\times$ County_ssa			-0.00475***		-0.00424**
			(-2.64)		(-2.39)
$\lambda\times$ D_Profit				0.980	1.327**
				(1.57)	(2.03)
Overall_rating	-0.188***	-0.182***	-0.188***	-0.191***	-0.185***
	(-4.70)	(-4.52)	(-4.68)	(-4.75)	(-4.58)
County FE	Yes	Yes	Yes	Yes	Yes
Observations	6478	6478	6478	6478	6478
R^2	0.078	0.079	0.079	0.078	0.080

Note: The dependant variable is the total number of COVID-19 Deaths in the nursing Home. t statistics in parentheses, * $p < 0.10$, ** $p < 0.05$, *** $p < 0.01$. Standard errors are robust to heteroscedasticity of unknown form.

Acknowledgments. We thank M.K. Chen et al. and all the team members of the Protect Nursing Homes project for generously sharing their data on U.S. nursing home networks. We express our gratitude to Editor Gregory Ponthiere and three anonymous referees for insightful and constructive comments that have helped improve our paper. We also acknowledge valuable suggestions from Randall Monty, Jakina Guzman, and seminar participants at the University of Kent, Université de Sherbrooke, the University of Texas Rio Grande Valley, and participants at the ASSA 2022 Annual Meeting, the European Meeting of the Econometric Society (EEA-ESEM virtual 2021), the Pan-African Scientific Research Council COVID-19 Conference, the 2021 China Meeting of the Econometric Society (CMES 2021), the 2021 Asian Meeting of the Econometric Society (AMES 2021), the 2021 Annual Conference of the Canadian Economics Association (CEA 2021), the 2021 Africa Meeting of the Econometric Society (AFES 2021), the 78th Annual Midwest Political Science Conference in 2021, and the 2020 Delhi Winter School of the Econometric Society (Winter School 2020). Special thanks are due to Landon Liu, Andrew Dormer, and Junior Sidie for excellent research assistance.

Declarations

Pongou acknowledges generous research support from the Government of Ontario under ERA grant 400201-190299-2001, the SSHRC's Partnership Engage Grants COVID-19 Special Initiative (PEG 231377-190299-2001), and the SSHRC's Insight Grant 231415-190299-2001. Guy Tchuente and Jean-Baptiste Tondji declare that they have no competing interests.

References

Acemoglu, D., Chernozhukov, V., Werning, I., Whinston, M.D. (2021). Optimal targeted lockdowns in a multigroup SIR model. *American Economic Review: Insights*, *3*(4), 487–502.

Adolph, C., Amano, K., Bang-Jensen, B., Fullman, N., Wilkerson, J. (2021). Pandemic politics: Timing state-level social distancing responses to COVID-19. *Journal of Health Politics, Policy and Law*, *46*(2), 211–233.

Alvarez, F.E., Argente, D., Lippi, F. (2021). A simple planning problem for COVID-19 lock-down, testing, and tracing. *American Economic Review: Insights*, *3*(3).

Anastassopoulou, C., Russo, L., Tsakris, A., Siettos, C. (2020). Data-based analysis, modelling and forecasting of the COVID-19 outbreak. *PloS One*, *15*(3), e0230405.

Anderson, R.M., & May, R.M. (1992). *Infectious diseases of humans: dynamics and control*. Oxford University Press.

Andreasen, V. (2011). The final size of an epidemic and its relation to the basic reproduction number. *Bulletin of Mathematical Biology*, *73*(10), 2305–2321.

Asavathiratham, C. (2001). *The influence model: A tractable representation for the dynamics of networked Markov chains* (Unpublished doctoral dissertation). Massachusetts Institute of Technology.

Baccini, L., & Brodeur, A. (2021). Explaining governors' response to the COVID-19 pandemic in the United States. *American Politics Research*, *49*(2), 215–220.

Baccini, L., Brodeur, A., Weymouth, S. (2021). The COVID-19 pandemic and the 2020 US presidential election. *Journal of Population Economics*, *34*(2), 739–767.

Ballester, C., Calvó-Armengol, A., Zenou, Y. (2006). Who's who in networks. wanted: The key player. *Econometrica*, *74*(5), 1403–1417.

Balmford, B., Annan, J.D., Hargreaves, J.C., Altoè, M., Bateman, I.J. (2020). Cross-country comparisons of covid-19: policy, politics and the price of life. *Environmental and Resource Economics*, *76*(4), 525–551.

Bandyopadhyay, S., Chatterjee, K., Das, K., Roy, J. (2021). Learning or habit formation? Optimal timing of lockdown for disease containment. *Journal of Mathematical Economics*, *93*, 102452.

Banerjee, A., Chandrasekhar, A.G., Duflo, E., Jackson, M.O. (2013). The diffusion of microfinance. *Science*, *341*(6144).

Barabási, A.-L., Albert, R., Jeong, H. (1999). Mean-field theory for scale-free random networks. *Physica A: Statistical Mechanics and its Applications*, *272*(1-2), 173–187.

Battiston, P., & Stanca, L. (2015). Boundedly rational opinion dynamics in social networks: Does indegree matter? *Journal of Economic Behavior*

& Organization, *119*, 400–421.

Berger, D., Herkenhoff, K., Huang, C., Mongey, S. (2020). Testing and reopening in an SEIR model. *Review of Economic Dynamics*, *In Press, Corrected Proof*.

Bethune, Z.A., & Korinek, A. (2020). *Covid-19 infection externalities: Trading off lives vs. livelihoods* (Working Paper No. 27009). National Bureau of Economic Research.

Bisin, A., & Moro, A. (2021). *Spatial-sir with network structure and behavior: Lockdown rules and the lucas critique* (Working Paper No. 28932). National Bureau of Economic Research.

Bosi, S., Camacho, C., Desmarchelier, D. (2021). Optimal lockdown in altruistic economies. *Journal of Mathematical Economics*, *93*, 102488.

Brauer, F. (2008). Epidemic models with heterogeneous mixing and treatment. *Bulletin of Mathematical Biology*, *70*(7), 1869.

Buchholz, K. (2020). *What share of the world population is already on covid-19 lockdown?* https://www.statista.com/chart/21240/enforced-covid-19-lockdowns-by-people-affected-per-country/. (Accessed: 2020-05-06)

Buechel, B., Hellmann, T., Klößner, S. (2015). Opinion dynamics and wisdom under conformity. *Journal of Economic Dynamics and Control*, *52*, 240–257.

Chang, S., Pierson, E., Koh, P.W., Gerardin, J., Redbird, B., Grusky, D., Leskovec, J. (2021). Mobility network models of COVID-19 explain inequities and inform reopening. *Nature*, *589*(7840), 82–87.

Chen, H.-F., & Karim, S.A. (2021). Relationship between political partisanship and covid-19 deaths: future implications for public health. *Journal of Public Health (Oxford, England)*.

Chen, M.K., Chevalier, J.A., Long, E.F. (2021). Nursing home staff networks and COVID-19. *Proceedings of the National Academy of Sciences*, *118*(1).

Conlen, M., Ivory, D., Yourish, K., Lai, R., Hassan, A., Calderone, J., et al. (2021). *Nearly one-third of U.S. coronavirus deaths are linked to nursing homes.* https://www.nytimes.com/interactive/2020/us/coronavirus-nursing-homes.html. (Accessed: 2020-10-14)

Debnam Guzman, J., Mabeu, M.C., Pongou, R. (2022). Identity during a crisis: COVID-19 and ethnic divisions in the United States. *AEA Papers and Proceedings 112*, *Forthcoming*.

Diekmann, O., Heesterbeek, J.A.P., Metz, J.A. (1990). On the definition and the computation of the basic reproduction ratio r 0 in models for infectious diseases in heterogeneous populations. *Journal of Mathematical Biology*, *28*(4), 365–382.

Douglas, P.H. (1976). The Cobb-Douglas production function once again: its history, its testing, and some new empirical values. *Journal of Political Economy*, *84*(5), 903–915.

Eichenbaum, M.S., Rebelo, S., Trabandt, M. (2021). The macroeconomics of epidemics. *The Review of Financial Studies*, *34*(11), 5149–5187.

Fajgelbaum, P.D., Khandelwal, A., Kim, W., Mantovani, C., Schaal, E. (2021). Optimal lockdown in a commuting network. *American Economic Review: Insights*, *3*(4), 503–22.

Federico, S., & Ferrari, G. (2020). Taming the spread of an epidemic by lockdown policies. *Journal of Mathematical Economics*, *93*, 102453.

Forneron, J.-J., & Ng, S. (2018). The ABC of simulation estimation with auxiliary statistics. *Journal of Econometrics*, *205*(1), 112–139.

Freed, M., Cubanski, J., Neuman, T., Kates, J., Michaud, J. (2020). *What share of people who have died of COVID-19 are 65 and older – and how does it vary by state?* https://www.kff.org/coronavirus-covid-19/issue-brief/what-share-of-people-who-have-died-of-covid-19-are-65-and-older-and-how-does-it-vary-by-state/. (Accessed: 2021-10-12)

Galeotti, A., Golub, B., Goyal, S. (2020). Targeting interventions in networks. *Econometrica*, *88*(6), 2445–2471.

Ganesh, A., Massoulié, L., Towsley, D. (2005). The effect of network topology on the spread of epidemics. *Proceedings ieee 24th annual joint conference of the ieee computer and communications societies.* (Vol. 2, pp. 1455–1466).

Garetto, M., Gong, W., Towsley, D. (2003). Modeling malware spreading dynamics. *Ieee infocom 2003. twenty-second annual joint conference of the ieee computer and communications societies (ieee cat. no. 03ch37428)* (Vol. 3, pp. 1869–1879).

Gertler, P.J., & Waldman, D.M. (1992). Quality-adjusted cost functions and policy evaluation in the nursing home industry. *Journal of Political Economy*, *100*(6), 1232–1256.

Gollier, C. (2020a). Cost–benefit analysis of age-specific deconfinement strategies. *Journal of Public Economic Theory*, *22*(6), 1746–1771.

Gollier, C. (2020b). Pandemic economics: optimal dynamic confinement under uncertainty and learning. *The Geneva Risk and Insurance Review*, *45*(2), 80–93.

Green, D.M., Kiss, I.Z., Kao, R.R. (2006). Parameterization of individual-based models: comparisons with deterministic mean-field models. *Journal of Theoretical Biology*, *239*(3), 289–297.

Harris, J.E. (2020, April). *The subways seeded the massive coronavirus epidemic in new york city* (Working Paper No. 27021). National Bureau of Economic Research. Retrieved from http://www.nber.org/papers/w27021 10.3386/w27021

Heap, S.P.H., Koop, C., Matakos, K., Unan, A., Weber, N. (2020, June). *Valuating health vs wealth: The effect of information and how this matters for covid-19 policymaking* (Article). VoxEU.org. Retrieved from https://voxeu.org/article/health-vs-wealth-trade-and-covid-19-policymaking

Hethcote, H.W. (2000). The mathematics of infectious diseases. *SIAM review*, *42*(4), 599–653.

Hethcote, H.W., & Yorke, J.A. (2014). *Gonorrhea transmission dynamics and control* (Vol. 56). Springer.

Hong, B., Bonczak, B.J., Gupta, A., Thorpe, L.E., Kontokosta, C.E. (2021). Exposure density and neighborhood disparities in COVID-19 infection risk. *Proceedings of the National Academy of Sciences*, *118*(13).

International Monetary Fund (2020). *World Economic Outlook: The Great Lockdown*. Washington, DC.

Karaivanov, A. (2020). A social network model of covid-19. *Plos One*, *15*(10), e0240878.

Keeling, M.J., & Eames, K.T. (2005). Networks and epidemic models. *Journal of the Royal Society Interface*, *2*(4), 295–307.

Kephart, J.O., & White, S.R. (1992). Directed-graph epidemiological models of computer viruses. *Computation: the micro and the macro view* (pp. 71–102). World Scientific.

Kermack, W.O., & McKendrick, A.G. (1927). A contribution to the mathematical theory of epidemics. *Proceedings of the Royal Society of London. Series A*, *115*(772), 700–721.

Kuchler, T., Russel, D., Stroebel, J. (2021). JUE Insight: The geographic spread of COVID-19 correlates with the structure of social networks as measured by Facebook. *Journal of Urban Economics*, 103314.

Liu, Y., & Rocklöv, J. (2021). The reproductive number of the delta variant of SARS-CoV-2 is far higher compared to the ancestral SARS-CoV-2 virus. *Journal of Travel Medicine*, *28*(7), 1–3.

Lloyd, A.L., Valeika, S., Cintrón-Arias, A. (2006). Infection dynamics on small-world networks. *Contemporary Mathematics*, *410*, 209–234.

Ma, L., Shapira, G., De Walque, D., Do, Q.-T., Friedman, J., Levchenko, A.A. (2021). *The intergenerational mortality tradeoff of covid-19 lockdown policies* (Working Paper No. 28925). National Bureau of Economic Research.

Marquez-Padilla, F., & Saavedra, B. (2022). The unintended effects of the COVID-19 pandemic and stay-at-home orders on abortions. *Journal of Population Economics*, *35*(1), 269–305.

National Center for Health Statistics (2020). *Provisional COVID-19 deaths by sex and age.* https://data.cdc.gov/NCHS/Provisional-COVID-19-Deaths-by-Sex-and-Age/9bhg-hcku. (Accessed: 2021-10-12)

Neelon, B., Mutiso, F., Mueller, N.T., Pearce, J.L., Benjamin-Neelon, S.E. (2021). Associations between governor political affiliation and COVID-19 cases, deaths, and testing in the US. *American Journal of Preventive Medicine*, *61*(1), 115–119.

Newman, M.E. (2002). Spread of epidemic disease on networks. *Physical Review E*, *66*(1), 016128.

Pastor-Satorras, R., Castellano, C., Van Mieghem, P., Vespignani, A. (2015). Epidemic processes in complex networks. *Reviews of Modern Physics*, *87*(3), 925.

Pastor-Satorras, R., & Vespignani, A. (2001). Epidemic spreading in scale-free networks. *Physical Review Letters*, *86*(14), 3200.

Peng, L., Yang, W., Zhang, D., Zhuge, C., Hong, L. (2020). Epidemic analysis of covid-19 in china by dynamical modeling. *arXiv preprint arXiv:2002.06563*.

Pestieau, P., & Ponthière, G. (2022). Optimal lockdown and social welfare. *Journal of Population Economics*, *35*(1), 241–268.

Pindyck, R.S. (2020). *Covid-19 and the welfare effects of reducing contagion* (Working Paper No. 27121). National Bureau of Economic Research.

Pongou, R., & Serrano, R. (2013). Fidelity networks and long-run trends in HIV/AIDS gender gaps. *American Economic Review*, *103*(3), 298–302.

Pongou, R., & Serrano, R. (2016). Volume of trade and dynamic network formation in two-sided economies. *Journal of Mathematical Economics*, *63*, 147–163.

Pongou, R., Tchuente, G., Tondji, J.-B. (2022). Laissez-faire, social networks, and race in a pandemic. *AEA Papers and Proceedings 112*, *Forthcoming*.

Pongou, R., & Tondji, J.-B. (2018). Valuing inputs under supply uncertainty: The bayesian Shapley value. *Games and Economic Behavior*, *108*, 206–224.

Powell, T., Bellin, E., Ehrlich, A.R. (2020). Older adults and COVID-19: the most vulnerable, the hardest hit. *Hastings Center Report*, *50*(3), 61–63.

Prem, K., Liu, Y., Russell, T.W., Kucharski, A.J., Eggo, R.M., Davies, N., ... others (2020). The effect of control strategies to reduce social mixing on outcomes of the COVID-19 epidemic in wuhan, China: a modelling study. *The Lancet Public Health*, *5*(5), e261–e270.

Reyes-Santías, F., Cordova-Arevalo, O., Rivo-Lopez, E. (2020). Using flexible regression models for calculating hospital's production functions. *BMC Health Services Research*, *20*(1), 1–11.

Rodrigues, F.A. (2019). Network centrality: an introduction. *A mathematical modeling approach from nonlinear dynamics to complex systems* (pp. 177–196). Springer.

Seierstad, A., & Sydsaeter, K. (1986). *Optimal control theory with economic applications*. Elsevier North-Holland, Inc.

Sorci, G., Faivre, B., Morand, S. (2020). Explaining among-country variation in COVID-19 case fatality rate. *Scientific reports*, *10*(1), 1–11.

Stiglitz, J. (2020, July). *Joseph stiglitz on priorities for the post-covid economy* (Opinion). World Economic Forum. Retrieved from https://www.weforum.org/agenda/2020/05/coronavirus-health-economy-global-survey/

Van den Driessche, P., & Watmough, J. (2002). Reproduction numbers and sub-threshold endemic equilibria for compartmental models of disease transmission. *Mathematical Biosciences*, *180*(1-2), 29–48.

Van Mieghem, P., Omic, J., Kooij, R. (2008). Virus spread in networks. *IEEE/ACM Transactions On Networking*, *17*(1), 1–14.

Wang, Y., Chakrabarti, D., Wang, C., Faloutsos, C. (2003). Epidemic spreading in real networks: An eigenvalue viewpoint. *22nd ieee international symposium on reliable distributed systems, 2003. proceedings.* (pp. 25–34).

Watts, D.J., & Strogatz, S.H. (1998). Collective dynamics of 'small-world' networks. *Nature*, *393*(6684), 440–442.

Wichmann, B., & Wichmann, R. (2020). Nonparametric estimation of a primary care production function in urban brazil. *Health Economics Review*, *10*(1), 1–10.

Yang, J. (2021). *Impact of the COVID-19 pandemic on older adults in the U.S.-statistics & facts.* https://www.statista.com/topics/8276/impact-of-the-covid-19-pandemic-on-older-adults-in-the-us/. (Accessed: 2020-10-14)

Young, H.P. (2009). Innovation diffusion in heterogeneous populations: Contagion, social influence, and social learning. *American Economic Review*, *99*(5), 1899–1924.

Young, H.P. (2011). The dynamics of social innovation. *Proceedings of the National Academy of Sciences*, *108*(Supplement 4), 21285–21291.